LASER INTERFEROMETER GRAVITATIONAL WAVE OBSERVATORY

LIGO Laboratory / LIGO Scientific Collaboration

LIGO-T1000339-v3 *ADVANCED LIGO* 11-Jan-11

HAM Auxiliary Suspensions Modeling and Test Results

Giacomo Ciani

Distribution of this document:
LIGO Science Collaboration

This is an internal working note
of the LIGO Project.

California Institute of Technology
LIGO Project – MS 18-34
1200 E. California Blvd.
Pasadena, CA 91125
Phone (626) 395-2129
Fax (626) 304-9834
E-mail: info@ligo.caltech.edu

Massachusetts Institute of Technology
LIGO Project – NW17-161
175 Albany St
Cambridge, MA 02139
Phone (617) 253-4824
Fax (617) 253-7014
E-mail: info@ligo.mit.edu

LIGO Hanford Observatory
P.O. Box 1970
Mail Stop S9-02
Richland WA 99352
Phone 509-372-8106
Fax 509-372-8137

LIGO Livingston Observatory
P.O. Box 940
Livingston, LA 70754
Phone 225-686-3100
Fax 225-686-7189

http://www.ligo.caltech.edu/

Contents

1 Introduction

1.1 Purpose

This document describes the modeling performed in support of the Ham Aux suspensions design, as well as the results of testing conducted on the first prototype.

1.2 Scope

This document covers the following topics:

- Analytical and FEA modeling of the blades.
- Modeling of the suspension chain using Mark Barton's Mathematica suspension toolbox.
- Measurement of the resonant frequencies of the 6 normal
- Measurement of the resonances quality factors, with particular interest in the Q obtained via eddy current passive damping

1.3 Acronyms

AOSEM	Another Optical Sensor Electromagnetic Motor
CoM	Center of Mass
DoF	Degree(s) of Freedom
HAM	Horizontal Access Module
HAM Aux	HAM Auxiliary Suspensions
SOS	Small Optics Suspension

1.4 Applicable Documents

1.4.1 LIGO Documents

LIGO-T1000526, "HAM Auxiliary Suspensions Design Requirements"

LIGO-T0900495, "HAM Auxiliary Suspensions Electronics Requirements"

LIGO-T1000338, "HAM Auxiliary Suspension Final design"

LIGO-D1000120, "ALIGO IO HAM AUX SUS ASSEMBLY"

LIGO-T1000351-v3, "Design Notes for Production Blades for HAM Suspensions"

LIGO-T0900561-v1, "Blade calculations for HSTS"

LIGO T1000100-v2, "Parametric Study of AOSEM Sensor Noise"

LIGO-T970135-02, "Small Optic Suspension Final Design"

LIGO-T0900285-v2, "L1 HAM6 ISI eLIGO Final Performance Measurements (March 24 2010)"

2 Modeling

2.1 General description

The HAM Aux suspension, described in LIGO-T1000338 and references therein, is shown in Figure 1.

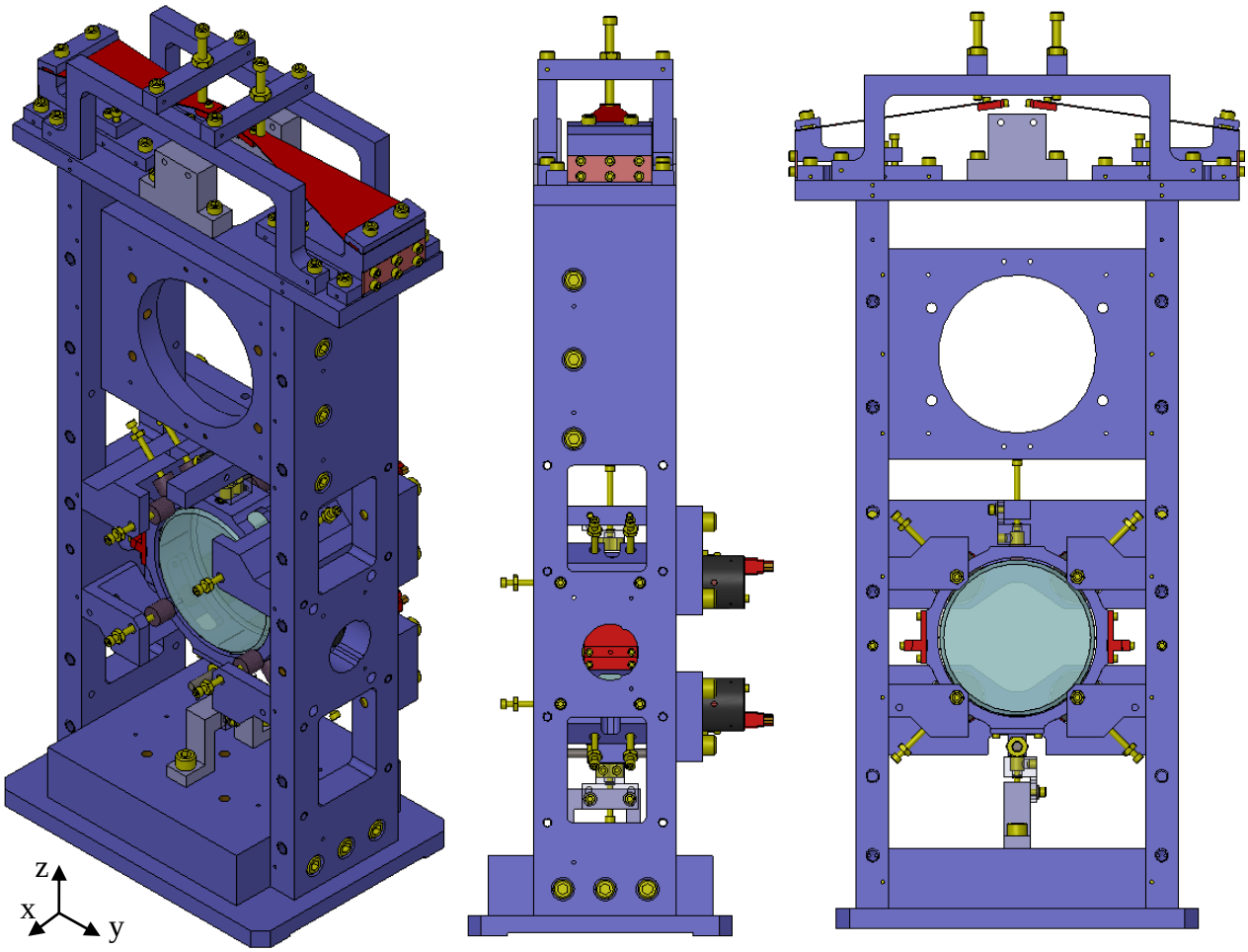

Figure 1. SolidWorks model of the HAM Aux Suspensions. Coordinate system is taken to have the x axis coincident with optic axis, pointing from the back of the suspension (the one with the AOSEMs) towards the front of the suspension (where the HR side of the optic is), and z one in vertical, pointing upwards (see the small axes at the left of the figure).

The suspension chain, illustrated in Figure 2, is schematized as follows:

- The upper wire suspension points are represented by the tips of two blades that provide vertical isolation. The blades are mounted such that under load the tips are horizontal and oscillates in the vertical direction.
- Two wires, one per side, depart from the blade tips and are clamped at the lower end to the side of an aluminum ring. On both the upper and lower attachment points, the wires departs from the clamps at the nominal angle, so that when the suspension is at rest the wires are completely straight.

- The aluminum ring hosts the 3” optic and all the auxiliary fixtures (clamps, magnets for the AOSEMs, etc…).
- Everything is symmetric with respect to a vertical plane containing the optic axis.

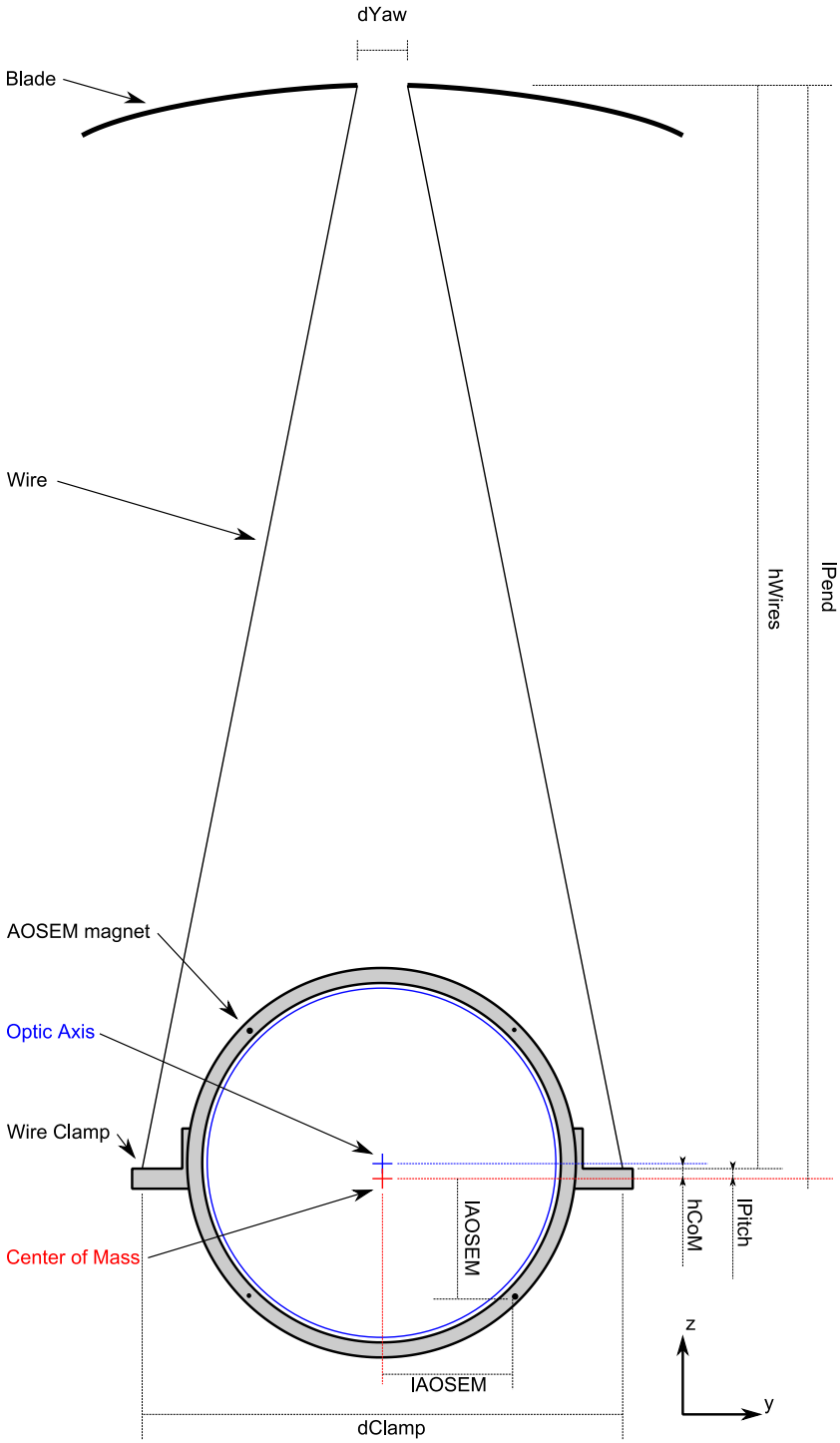

Figure 2. A schematic of the suspension chain showing relevant parameters. The blue circle represents the optic, and the blue cross it center. The surrounding grey ring is the optic’s

holder. The four small circles around the optics represent the position of the AOSEMs magnets. The red cross is the suspended assembly center of mass. Upper and lower ending points of the wires represent the blade tips in nominal (loaded) position and the wire break-off points at the optic barrel, respectively.

2.2 Blades modeling

The Mathematica model used to calculate the suspension resonant modes (see 2.3) assumes that the blades are ideal springs acting in vertical, the spring constant being an input parameter to the model.

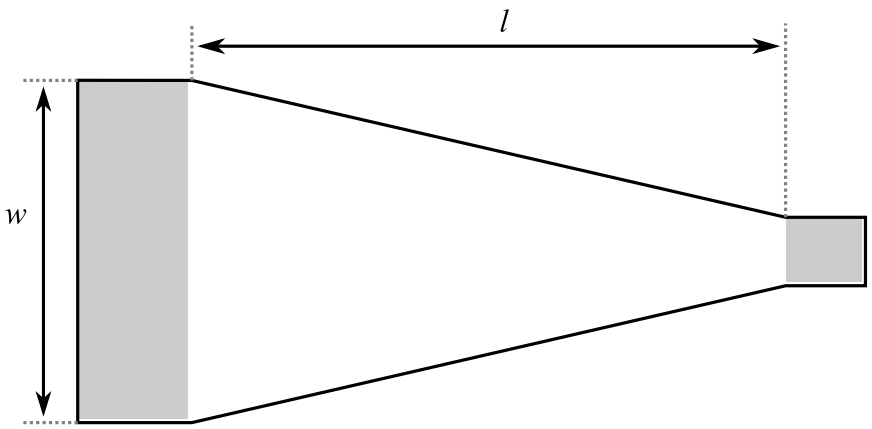

Figure 3. Approximate shape of the blades employed in the Ham Aux suspensions. The only part that actually flexes is the white one. The grey area on the left is clamped in the suspension structure; while the grey area on the right is superimposed and attached to a much ticker (3.6 mm) piece of metal, constituting the clamp for the wire, thus being basically rigid compare to the rest of the blade.

To calculate the spring constant expected for a given geometry (shown in Figure 3) and material, and to dimension the blades such as to be sure that the maximum stress would not exceed 50% of the material yield strength (as recommended by the suspension working group), two different approaches have been used. They are described in the following paragraphs.

2.2.1 Analytical model

Analytical formulae to calculate the bending, resonant frequency and maximum stress of a trapezoidal beam constrained at one end and with a load on the other end are known and used by the suspension working group to model the blades of different suspensions (see LIGO-T1000351-v3 and references therein). These formulae have been used by Norna Robertson to create a spreadsheet that, given the blade geometry, the material properties and the applied load, calculates the resulting bending and the resonance frequency, together with the maximum stress on the material (LIGO-T0900561-v1). A so called “shape factor” appears in all these formulae, and is related to the aspect ratio of the blades in a somewhat complicated fashion, thus bringing some uncertainty in the model itself. We used a shape factor of 1.54, found by the suspension group to reproduce quite well experimental results on blades with a shape similar to ours.

After a few iterations, the following material and geometry have been chosen for the blades (see Figure 3 for reference):

- Stainless Steel 304
  - Young's modulus: 200 GPa (nominal)
  - Yield strength: 215 MPa (nominal)
- Width at major base (*w*): 40.6 mm
- Length of the flexing portion part (*l*): 76.8 mm
- Thickness (uniform): 0.020"[1].

2.2.2 FEA model

Given the uncertainty introduced by the not-well-known shape factor, the geometry obtained by the analytical calculation has been modeled in COMSOL Multiphysics using the Structural Mechanics Module.

The exact shape of the blade has been modeled, including the clamped part and the thickest part at the tip (see Figure 4). Moreover, as in the suspension the wire leaves the tip at an angle of about 106 deg, in the COMSOL model the force is applied on the tip at the right angle, instead of orthogonal to the blade as assumed by the analytical model.

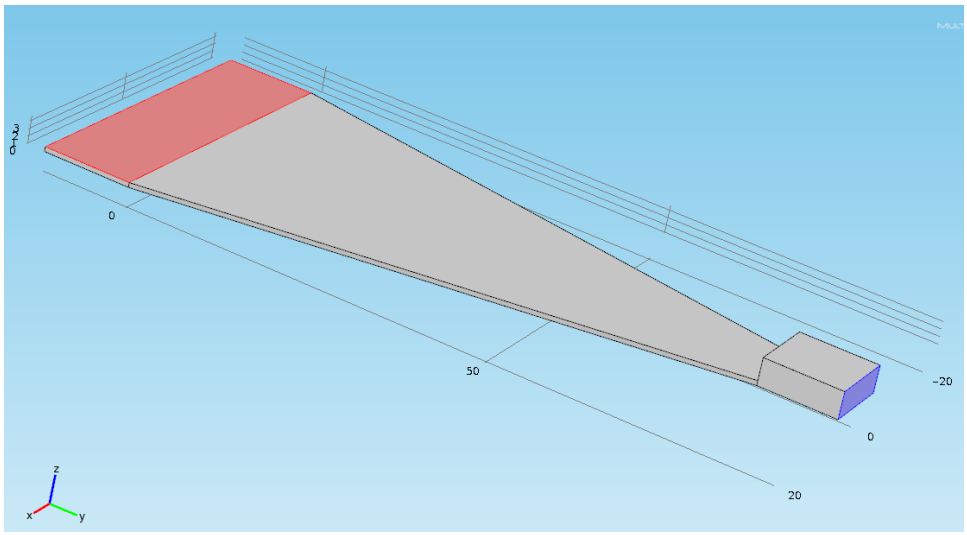

Figure 4. The geometry used in the COMSOL model (here upside down). The red face and the corresponding one on the other side of the model (not visible) are treated as fixed (they are clamped in the support structure). The load is applied to the blue face at an angle of 106 deg with respect to the face normal, towards the positive z axis and negative y axis in the model. Using the face normal as a reference assures that the force will act in the right direction regardless of the final bending of the blade. In fact in the real suspension the blade angle at the base will be adjusted so that under load the tip will be horizontal (blue face vertical), and the wire will depart at 106 deg.

[1] During modeling, 0.025" have been considered too, but we settled on 0.020".

A static analysis has been performed on the model, obtaining the displacement of the tip under load and the maximum material stress in the blade, as shown in Figure 5.

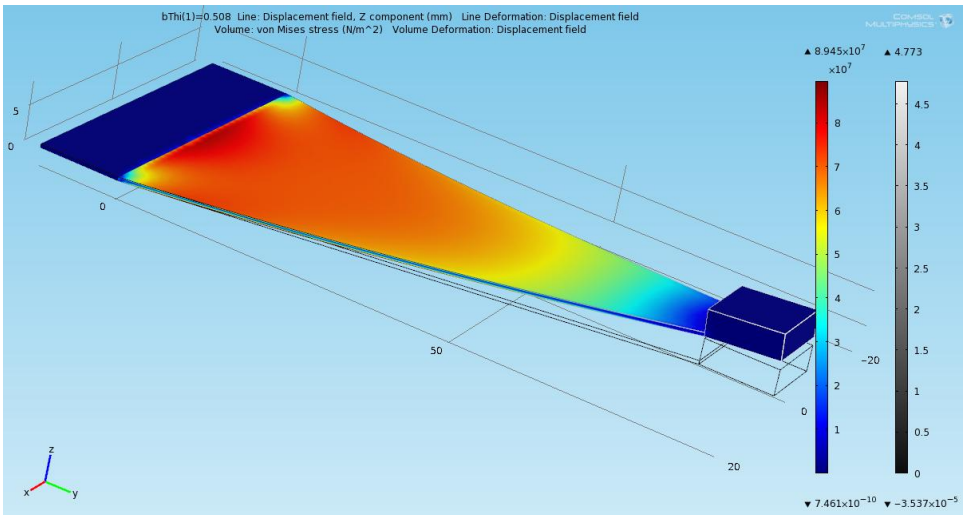

Figure 5. The result of the FEA modeling for a blade thickness of 0.020". The rainbow coloring, corresponding to the leftmost scale, represents the material stress. The rightmost scale corresponds to the displacement and has the only purpose of showing the maximum value of 4.77 mm, occurring at the tip. The colored model is deformed according to the result of the calculation, while the grey wireframe represent the straight unloaded blade.

2.2.3 Results comparison

Both the analytical and the FEA models have been used to obtain the maximum stress and the tip displacement under load. Then, the spring constant has been calculated as $k = mg/dx$, where m is the suspended mass, g the gravity acceleration and dx the tip displacement. The estimated bounce frequency (not accounting for the elasticity of the wires) can be estimated as $f = (k/m)^{1/2}/(2 \cdot \pi)$. Table 1 compares the results obtained with the analytical and FEA models for blades of thickness 0.020" and 0.025".

Table 1. Blades properties as obtained by the two model. The level of agreement is very good.

Blade type	***Thickness = 0.020"***		***Thickness = 0.025"***	
Model	***Analytical***	***FEA***	***Analytical***	***FEA***
Maximum stress (MPa)	81	89	52	57
Vertical displacement (mm)	4.81	4.77	2.46	2.46
Spring constant (N/m)	381	384	745	745
Resonant frequency (Hz)	7.19	7.19	10.05	10.05

The agreement between the two models is very good, with the FEA modeling giving slightly higher (10%) values for the maximum stress in the material. The 0.020" blade seems to achieve reasonable stress (below 50% of the maximum value of 215 MPa) while still keeping the resonance below the LIGO measurement band. Unfortunately, measured quantities on actual blades prototypes don't agree that well with the modeled values (see section 3.2).

2.3 Mathematica model

The suspension chain has been modeled using Mark Barton's Mathematica suspension toolbox. The toolbox allows for modeling the entire suspension system, extracting the normal modes together with their frequencies. It also calculates the transfer functions between suspension structure degrees of freedom and optics degrees of freedom.

2.3.1 Model definition

The model of the suspension comprises the following elements:

- Blades: they are treated as ideal unidirectional mass-less springs to which the wires are attached. The only parameters associated with them are the spring constant that is obtained by separate modeling (see 2.2), and the horizontal distance between the tips. The blade tips are also considered to be mass-less.
- Wires: besides the length, diameter and materials properties are included to account for the effect of elasticity and flexure points. They are considered mass-less.
- Suspended assembly: considered a single object, the relevant parameters are mass, moment of inertia, wires attaching points and CoM positions in the local coordinate system. The origin of this system is in at the intersection between the axis of the optic and the plane containing the wires, with the x axis parallel to the axis of the optics and the z one in vertical.

The global coordinate system axes are parallel to those of the suspended assembly local coordinate system.

Table 2 lists all the parameters used in the model, their values and how they were obtained ()

Table 2. Parameters used in the Mathematica model. Meaning of the "Source" column is as follows: "by design" = design driver; "derived" = calculated from the value of other parameters; "SolidWorks" = calculated by SolidWorks based on the solid model; "vendor specs" = the value is obtained by data sheets or equivalent documentation; "separate modeling" = the value used here is obtained by a modeling described somewhere else in this document.

Name	***Description***	***Source***	***Value***
m0	Mass of suspended assembly	SolidWorks model	.3738 Kg
I0x	Moments of inertia of the suspended assembly with respect to the axis of the local coordinate system (x, y and z respectively)	SolidWorks model	$2.12 \cdot 10^{-4}$ Kg·m^2
I0y			$2.69 \cdot 10^{-4}$ Kg·m^2
I0z			$4.35 \cdot 10^{-4}$ Kg·m^2
COMx	Coordinates of the suspended assembly center of mass in local coordinates	SolidWorks model	0 mm
COMy			0 mm
COMz			-2.65 mm
tl0	Vertical distance between upper and lower wires attachment points (hWires in Figure 2)	By design	249.3 mm
l0	Wires length	Derived	252.9 mm

dyaw1	Horizontal separation of wires attachment points at blade tips (dYaw in Figure 2)	By design	15.7 mm
dyaw2	Horizontal separation of wires attachment points at suspended (hClamp in Figure 2)	By design	100.3 mm
Dpitch	y coordinate of lower wires attachment points with respect to optic axis (hCoM-lPitch in Figure 2)	By design	-1.65 mm
r0	Radius of wires	Vendor specs	0.076 mm
Y0	Young's modulus of wires' steel	Vendor specs	210 GPa
Kbz	Blades' stiffness	Separate modeling	392 N/m

2.3.2 Normal modes

The suspended assembly is the only massive object and is treated as a rigid body. Therefore there are six degrees of freedom. They are at least partially mixed in an equal number of normal modes. Indeed, the x and pitch DoF of the optic give rise to two normal modes, the y and roll to other two, while the yaw and bounce have their own independent motion. Table 3 lists the normal modes of the suspension chain and their frequencies, as obtained from the Mathematica model.

Table 3. Modeled modes of the Ham Aux suspension and corresponding frequencies

Name	***Description***	***Value***
fPitch1	Frequency of first pitch/x normal mode	0.98 Hz
fPitch2	Frequency of second pitch/x normal mode	1.12 Hz
fYaw	Frequency of yaw mode	0.76 Hz
fBounce	Frequency of vertical motion	7.19 Hz
fRoll1	Frequency of first roll/y normal mode	1.00 Hz
fRoll2	Frequency of second roll/y normal mode	10.63 Hz

2.3.3 Transfer functions

As far as the model is concerned, the only coupling of the optic to the environment is trough movement of the support structure, i.e. the upper suspension points.

The calculated transfer functions between excitations of the support structure and the optic DoFs are obtained from the model and plotted in Figure 6 through Figure 15. The angular coordinates of the structure are worth a clarification: you may be tempted to assume that the rotation is around some point at the base of the suspension, and thus a pitch of the structure, for example, will cause the upper suspension point to be translated in x, obviously exciting the optic. However, this would be somehow arbitrary and it is not the way the model is implemented: the pivoting point is supposed to be a point half way between the two upper suspension points in their nominal position. In this case, a pitch of the structure will just be a change in the angle (in the x-z plane) at which the wires leaves the suspension point. This couples to the pitch and x DoFs of the optic only because the rigidity of the wire and the variation of load on the blades, that the model does take into account.

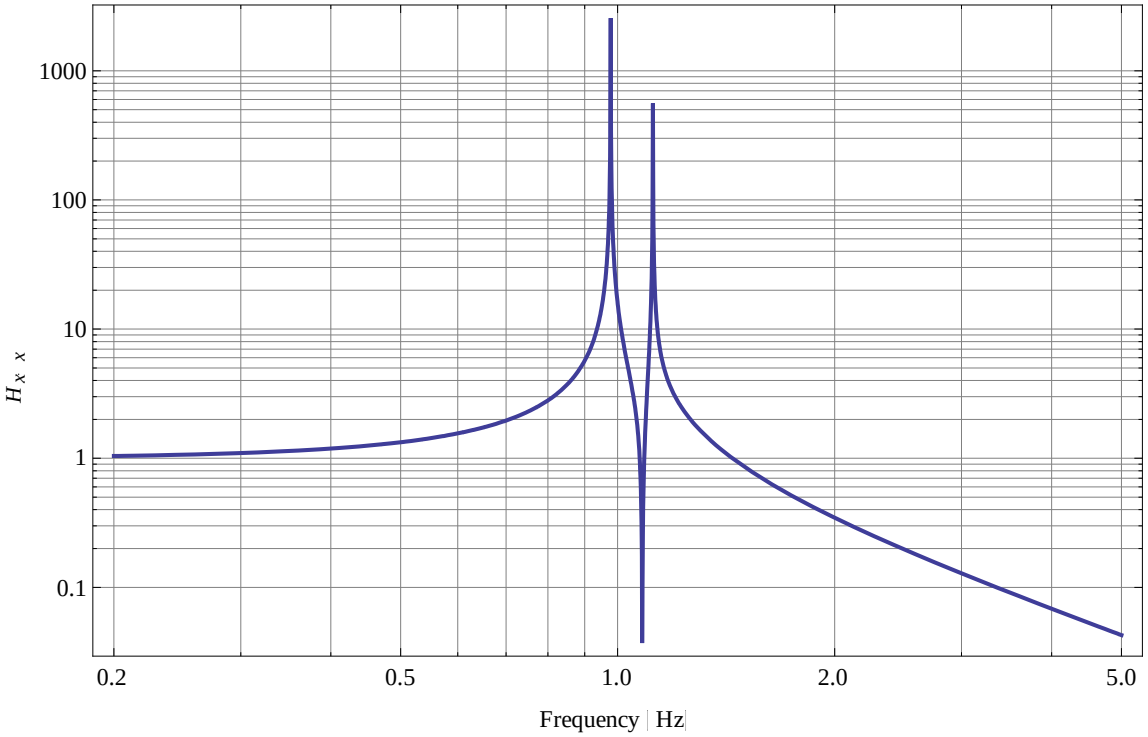

Figure 6. x to x transfer function.

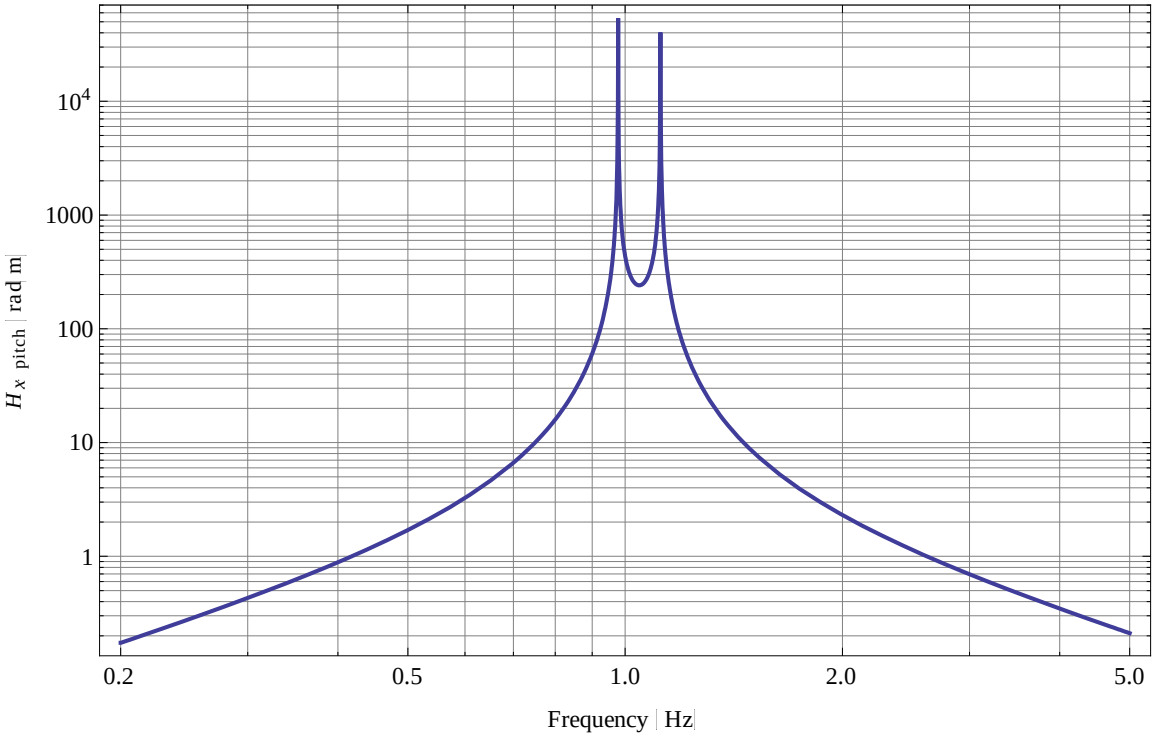

Figure 7. x to pitch transfer function.

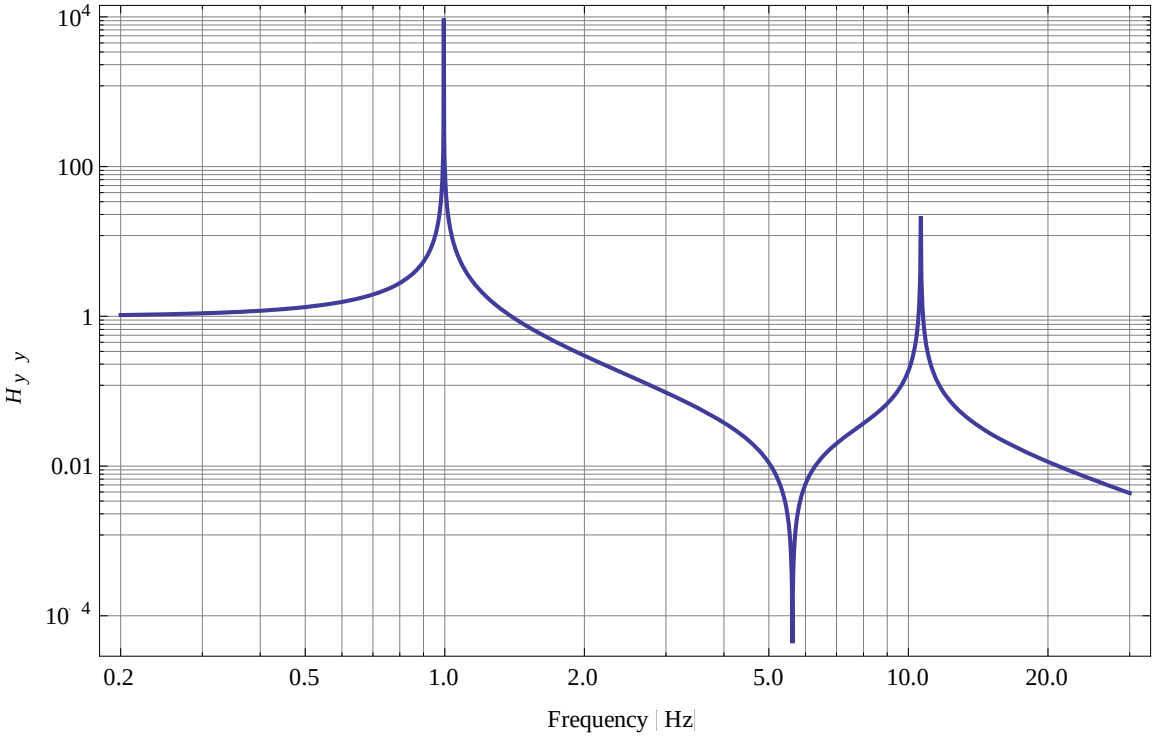

Figure 8. y to y transfer function

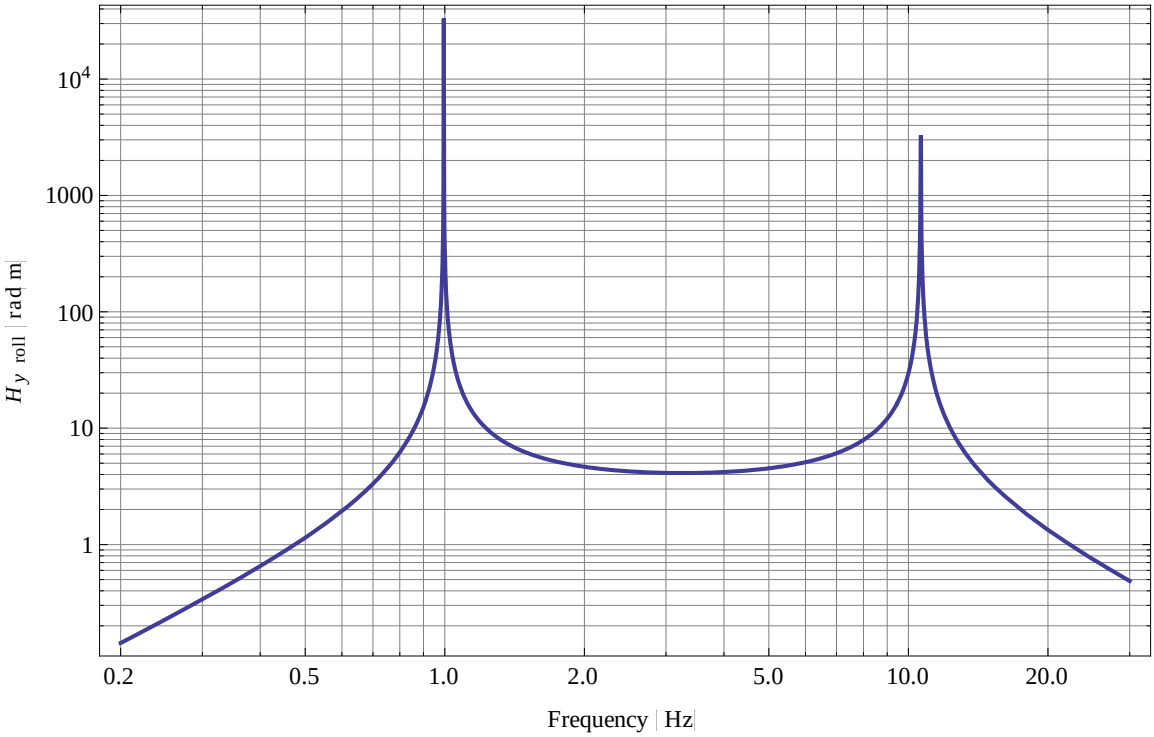

Figure 9. y to roll transfer function

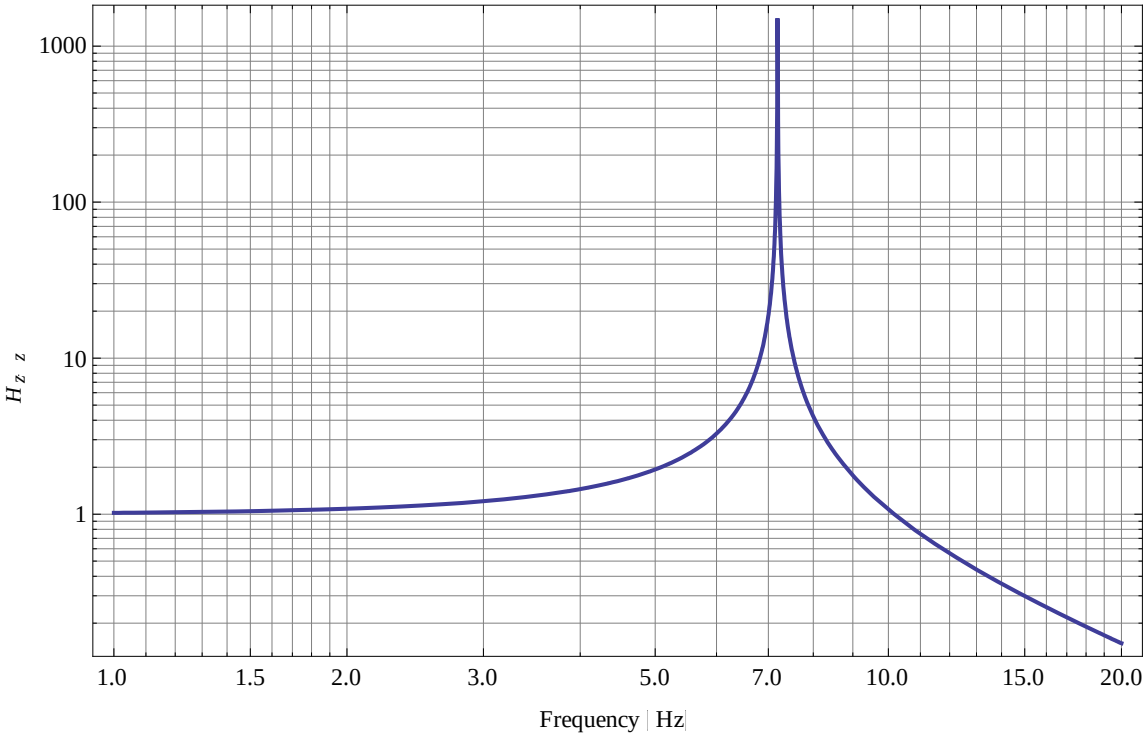

Figure 10. z to z transfer function

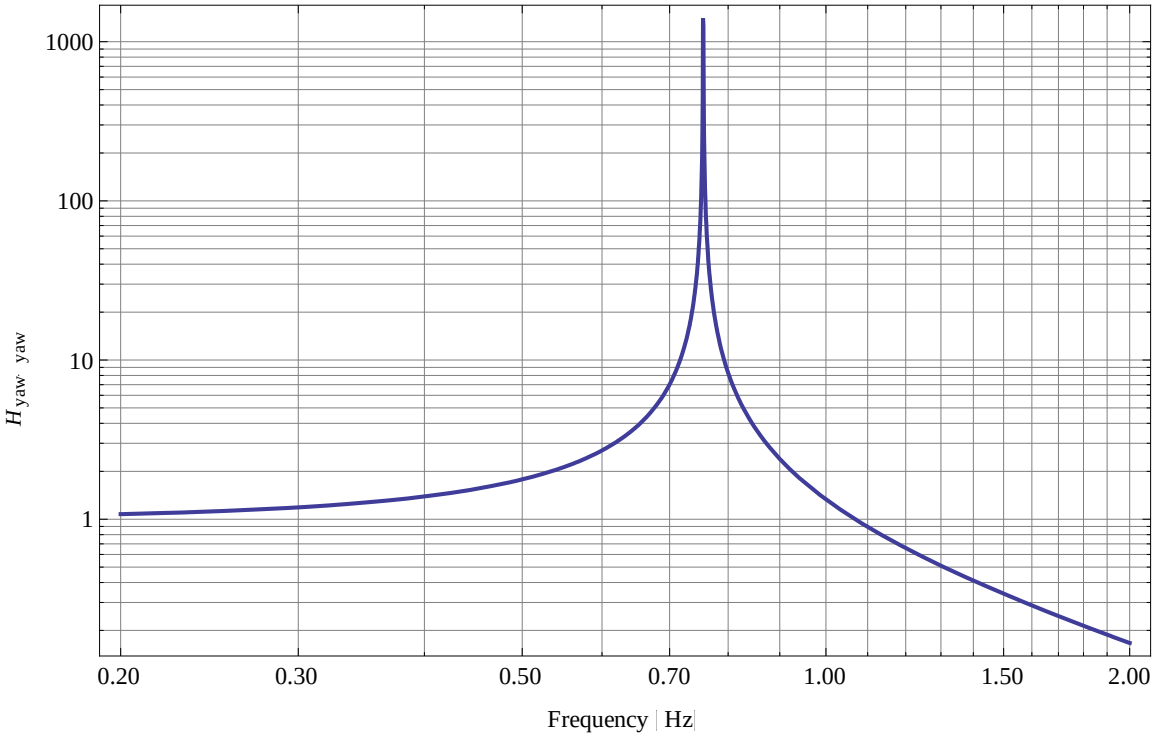

Figure 11. Yaw to yaw transfer function

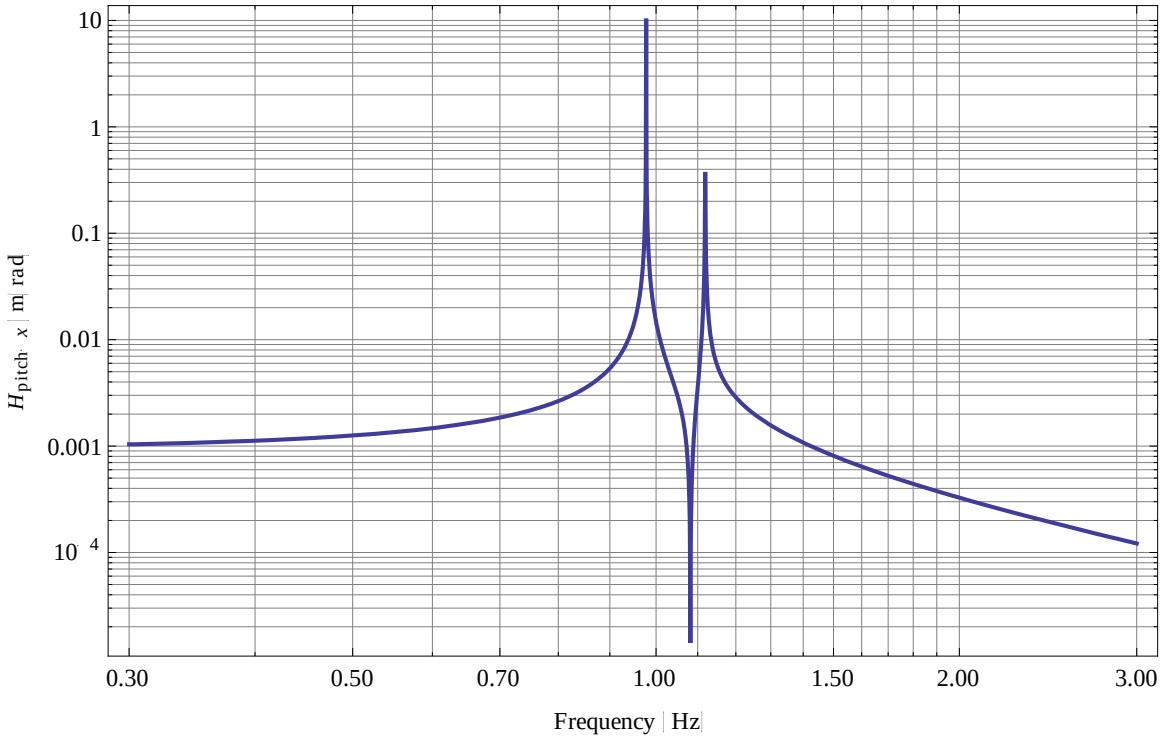

Figure 12. Pitch to x transfer function.

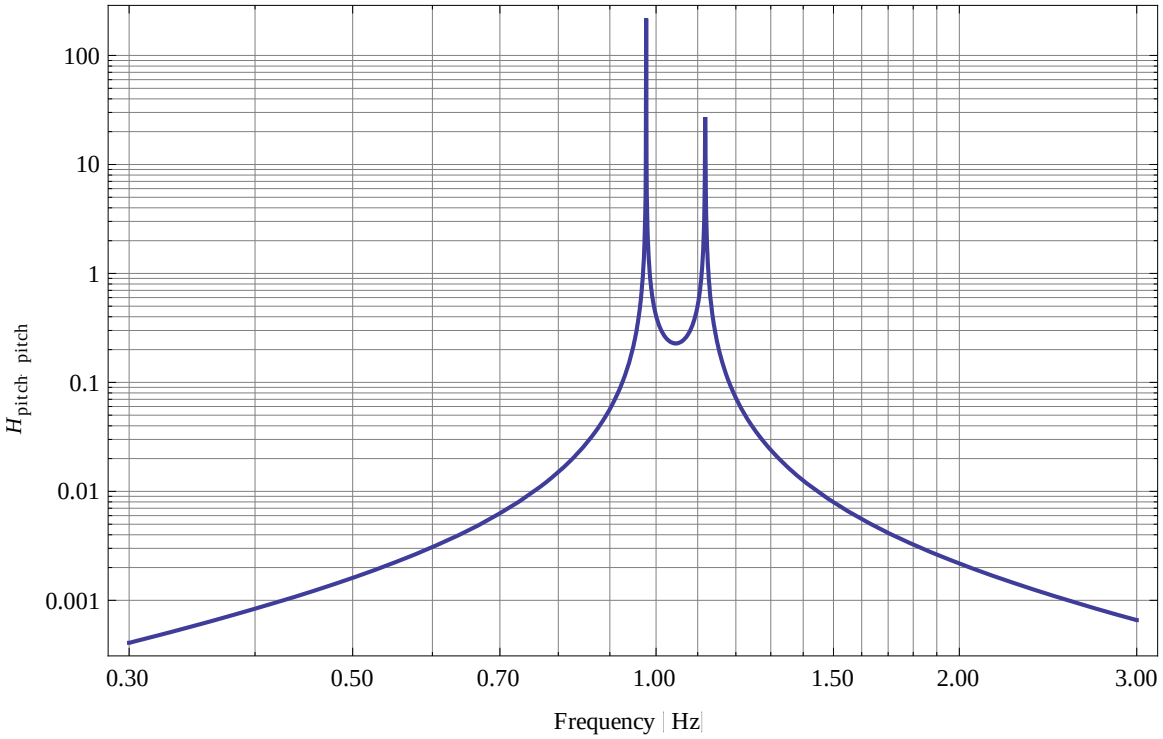

Figure 13. Pitch to pitch transfer function.

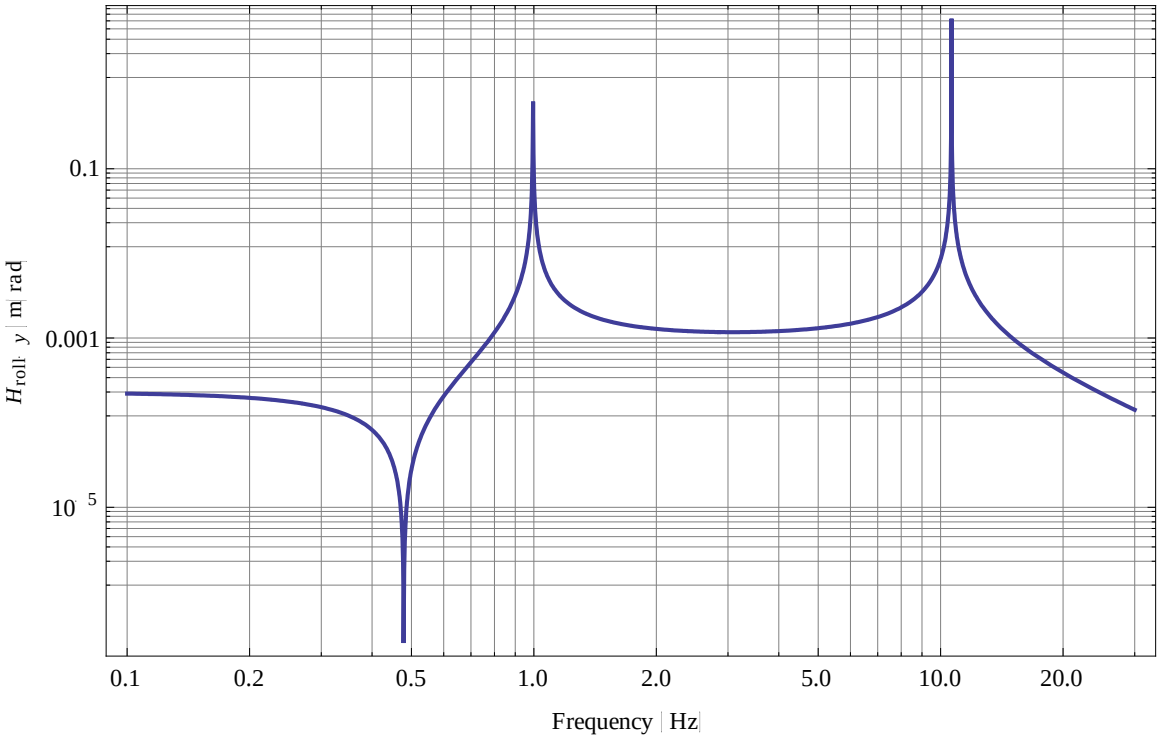

Figure 14. Roll to y transfer function.

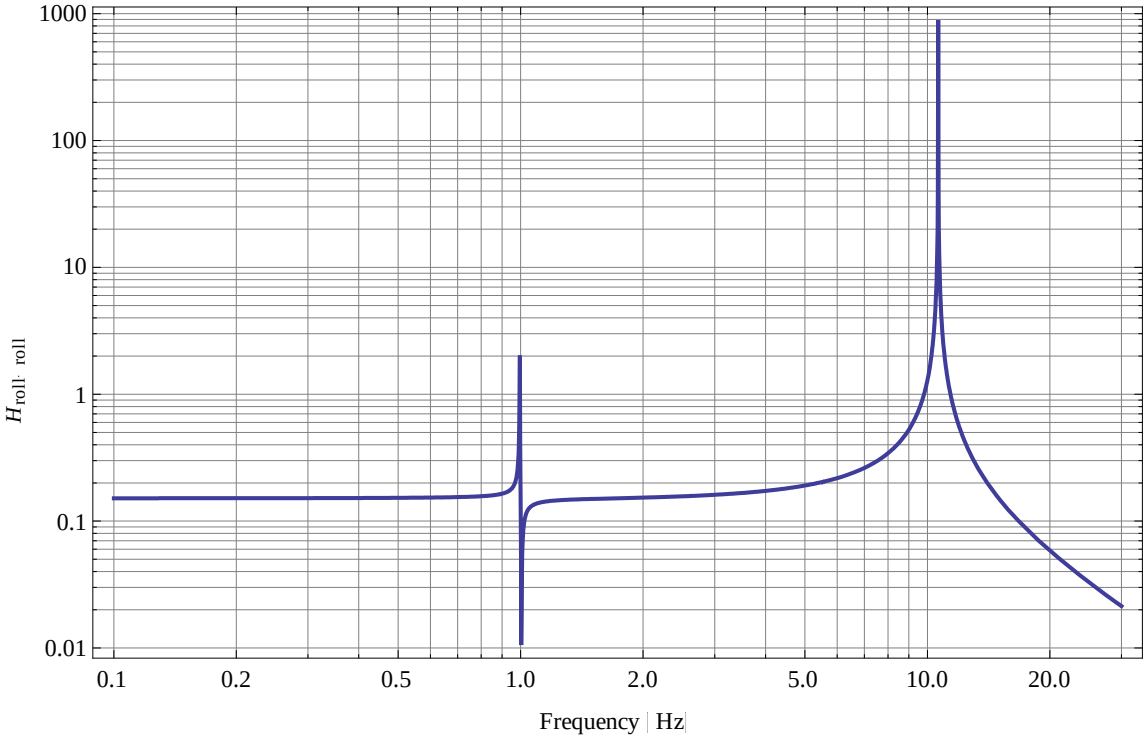

Figure 15. Roll to roll transfer function.

2.3.4 Noise and damping

While it is desirable to lower the noise in all degrees of freedom to reduce the risk of spurious couplings, pitch and yaw are the only ones that nominally affect the beam jittering. Also, noise in the x DoF can directly affect the laser phase noise (see requirement expressed in LIGO-T1000526). Moreover, these three DoF are actively controlled using the AOSEMs both for DC pointing and active damping of the resonances.

To estimate the noise performance and check compliance with the requirements, a noise model based on the transfer function calculated with Mathematica has been developed for each of these DoF accounting for the major sources of noise; also, a simple feedback loop has been inserted in the model: while this will most likely not be the actual implementation of the control loop, it serves to show that the requirements can be met, and to analyze the role of the different noise sources.

In looking at the noise spectra the reader should keep in mind that, in the cases were the gain of the control loop is set to 0 and thus the resonances are not damped, the reported RMS value is greatly underestimated. This is due to the fact that the resolution of the experimental spectrum is too low to resolve the sharp resonances. However, the limited resolution is only due to the input noise data and not the transfer functions itself that are available from the model with arbitrary precision. The effect can thus be estimated by comparing the integral of one of the transfer functions performed with very high resolution with the same integral performed at the resolution of the input noise data. While this number is much bigger than 1 in all cases in which the gain is 0, it is almost 1 for all the other presented values of the gain. In those cases we can consider the projected RMS value reliable.

2.3.5 Pitch noise

A scheme of the noise model for the pitch DoF is presented in Figure 16.

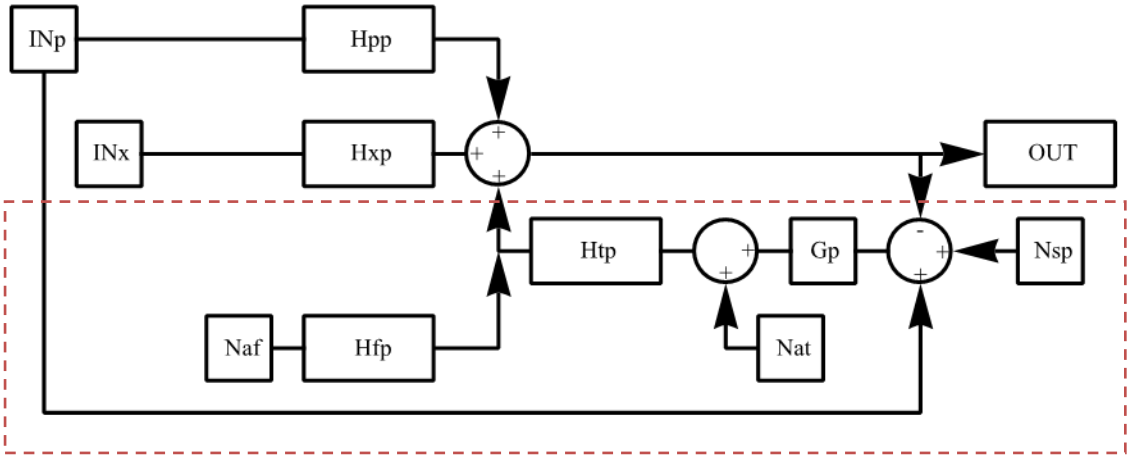

Figure 16. A scheme of the pitch noise model (see text for meaning of the acronyms). The part enclosed in the red dashed rectangle represents the effect of the AOSEMs and of the feedback loop. Also note that the position signal driving the feedback loop is the difference between the pitch of the optic and that of the structure, as the AOSEMs are mounted on the structure itself.

Abbreviations used in the scheme are defined as follows:

- Hpp: transfer function between suspension pitch and pitch of the optic
- Hpx: transfer function between suspension pitch and displacement of the optic
- Htp: transfer function between torque on the optic (y component) and pitch of the optic
- Hfp: transfer function between force on the optic (x component) and pitch of the optic
- INp: suspension structure pitch noise
- INx: suspension structure x noise
- Naf: force noise coming from the AOSEMs array
- Nat: torque noise coming from the AOSEMs array
- Nsp: pitch sensing noise of the AOSEMs array
- Gp: gain of the control loop (for the pitch DoF)

The corresponding output is:

$$\frac{(\mathrm{Hpp} + \mathrm{Gp\ Htp})}{1 + \mathrm{Gp\ Htp}}\mathrm{INp} + \frac{\mathrm{Hxp}}{1 + \mathrm{Gp\ Htp}}\mathrm{INx} + \frac{\mathrm{Hfp}}{1 + \mathrm{Gp\ Htp}}\mathrm{Naf} + \frac{\mathrm{Htp}}{1 + \mathrm{Gp\ Htp}}\mathrm{Nat} + \frac{\mathrm{GpHtp}}{1 + \mathrm{Gp\ Htp}}\mathrm{Nsp}$$

The noise spectra for INp and INx have been assumed to be equal to the expected HAM ISI noise spectra (see LIGO-T0900285-v2), as the suspension structure is rigidly attached to the table. For the AOSEMs sensing and actuation noise, requirements have been expressed in LIGO-T0900495 accounting for performances measured in the past for similar devices (see LIGO T1000100-v2). For the example control loop gain, the following function has been chosen:

$$Gx(\omega) = k\frac{2\,\pi\,z1 + i\,\omega}{(2\,\pi\,p1 + i\,\omega)(2\,\pi\,p2 + i\,\omega)}, \qquad z1 = 0.2\ Hz, \qquad p1 = 3\ Hz, \qquad p2 = 30\ Hz$$

Figure 17 through Figure 19 illustrate the projected pitch noise for three different values of the constant k in the feedback loop gain, including zero. They also show the contributions coming from the different noise sources, and the different role they play as the gain of the feedback loop is changed. Total noise spectra obtained in the three cases, expressed in terms of TEM10 mode amplitude, are compared in Figure 20.

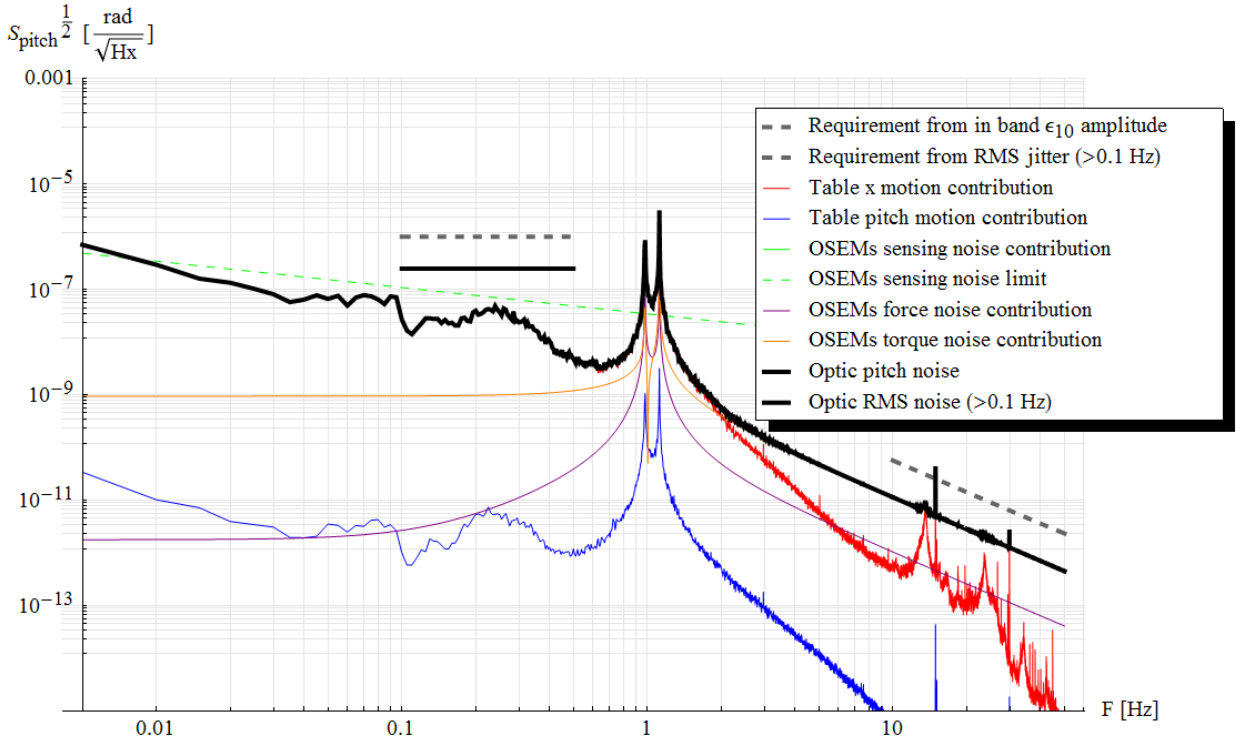

Figure 17. Projected pitch noise calculated using the Mathematica model with the control loop gain Gp set to zero. Contributions from individual noise sources are also shown. The flat short lines represent the RMS noise value (solid) and requirement (dashed) for f > 0.1 Hz. Note that the value of the RMS in this case (gain = 0) is greatly underestimated (see text).

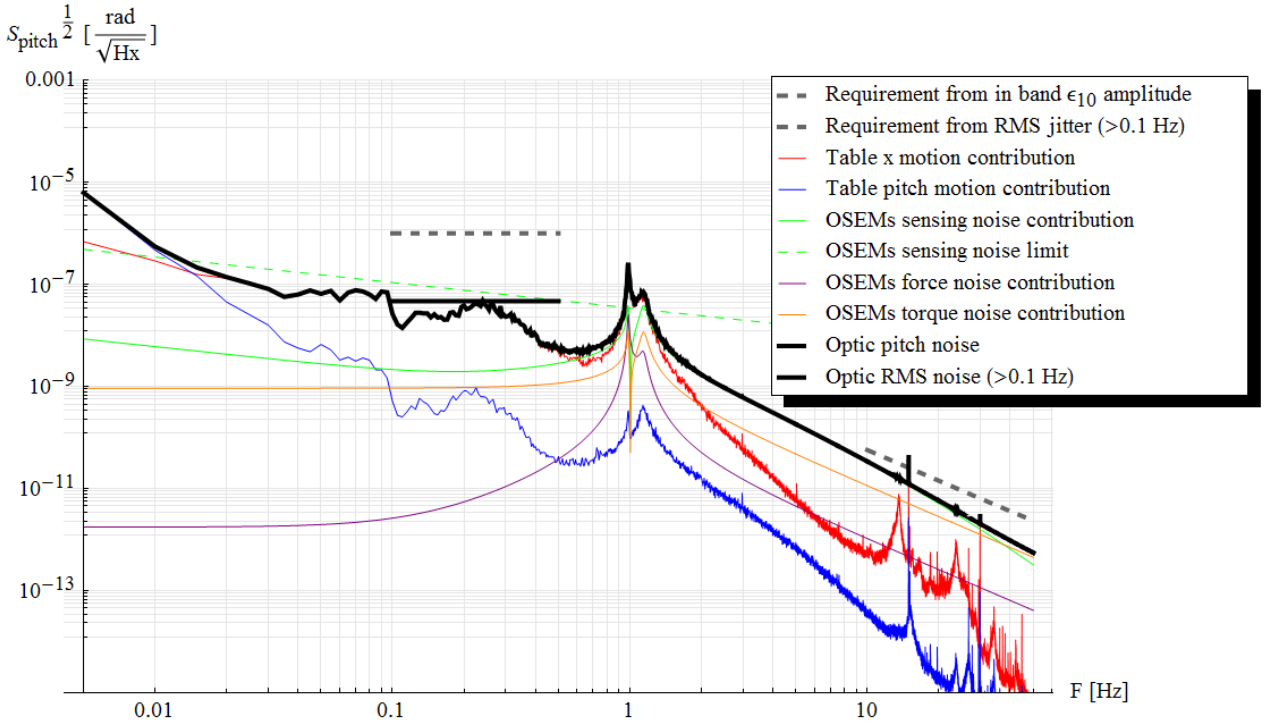

Figure 18. As Figure 17, but with the constant k in the control loop gain set to 0.5 (N m)/rad.

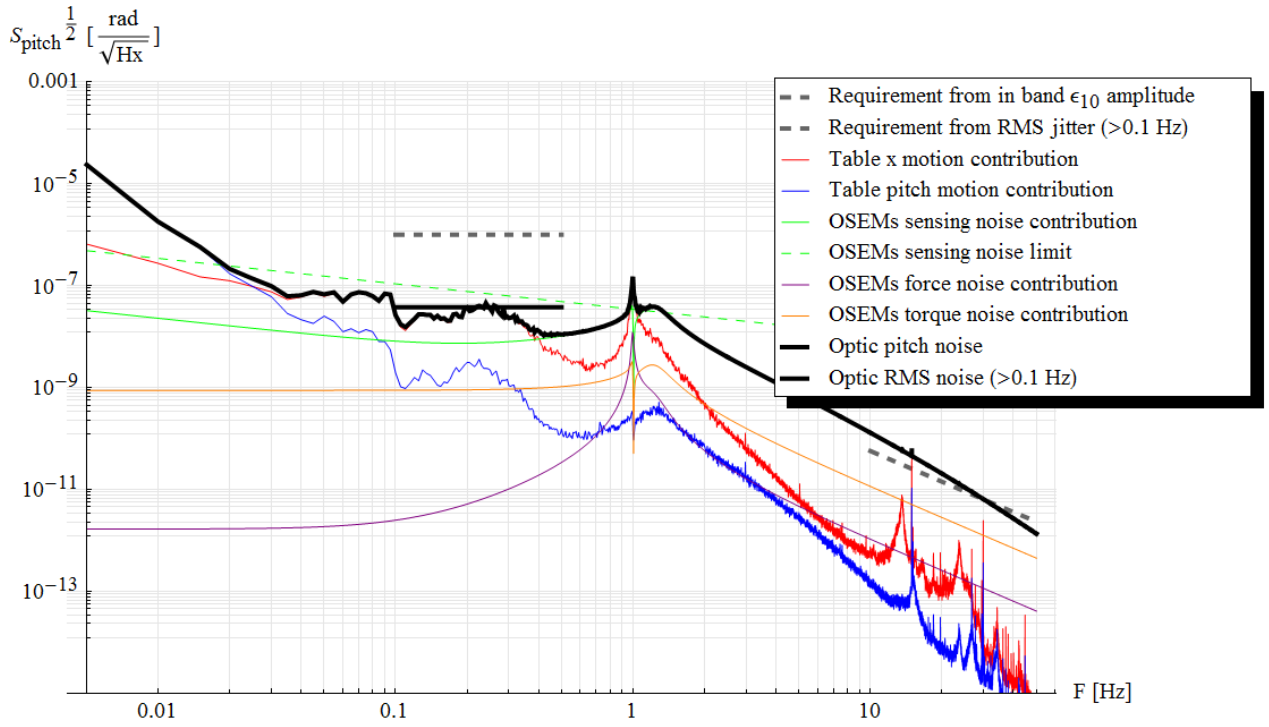

Figure 19. As Figure 17, but with the constant k in the control loop gain set to 2 (N m)/rad .

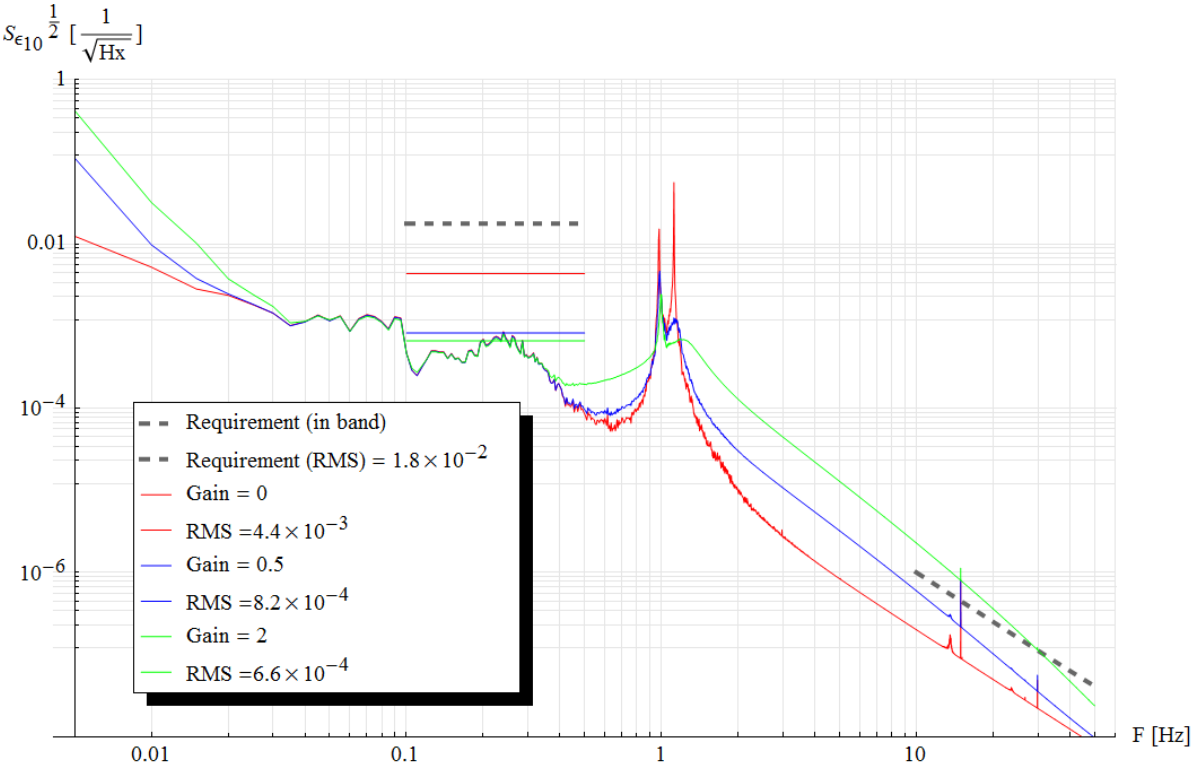

Figure 20. A comparison of the total TEM10 amplitude noise spectra due to the pitch motion of the optic. The colors represent the three different gain settings shown in previous figures. Note that the value of the RMS in the case of gain = 0 is greatly underestimated (see text).

2.3.6 Yaw noise

The noise model for the yaw DoF, schematized in Figure 21, is simpler than the one describing the pitch noise. In fact, there is no cross coupling between yaw and other DoF, with respect to both movement of the structure or forces/torques applied to the optic.

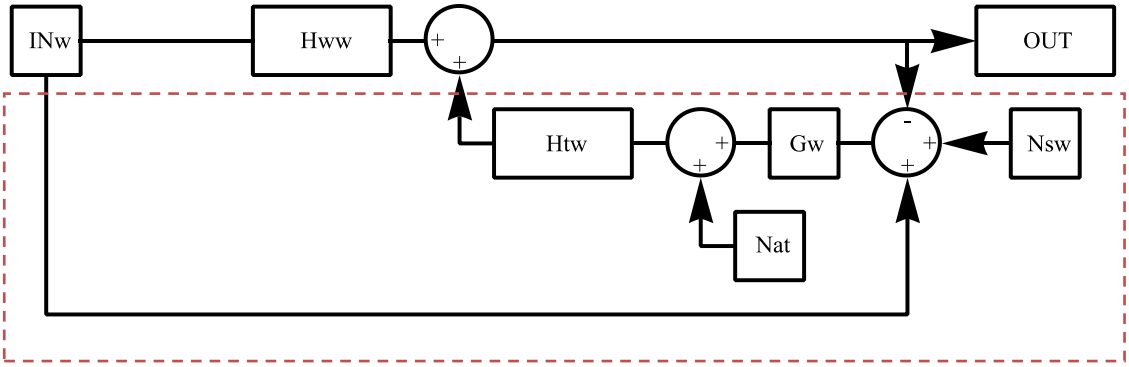

Figure 21. A schematic of the noise model for the yaw DoF. The only sources of noise nominally coupling with yaw DoF are the yaw of the structure and the torque noise of the AOSEMs. Same considerations as Figure 16 apply.

Abbreviations not already explained in the previous paragraph are as follow:

- Hww: transfer function between yaw of the structure and that of the optic
- Htw in the transfer function between torque applied to the optic (z component) and yaw of the optic
- INw: suspension structure yaw noise
- Nsw: yaw sensing noise of the AOSEMs array
- Gw: gain of the control loop (for the yaw DoF)

The output is:

$$\frac{(\mathrm{Gw\ Htw} + \mathrm{Hww})}{1 + \mathrm{Gw\ Htw}}\mathrm{INw} + \frac{\mathrm{Htw}}{1 + \mathrm{Gw\ Htw}}\mathrm{Nat} + \frac{\mathrm{Gw\ Htw}}{1 + \mathrm{Gw\ Htw}}\mathrm{Nsw}$$

The same sources of data as for the pitch have been used for INw and Nsw. The same control lopp function has also been used.

Figure 22 through Figure 24 are the analogous of Figure 17 through Figure 19, but for the yaw noise.

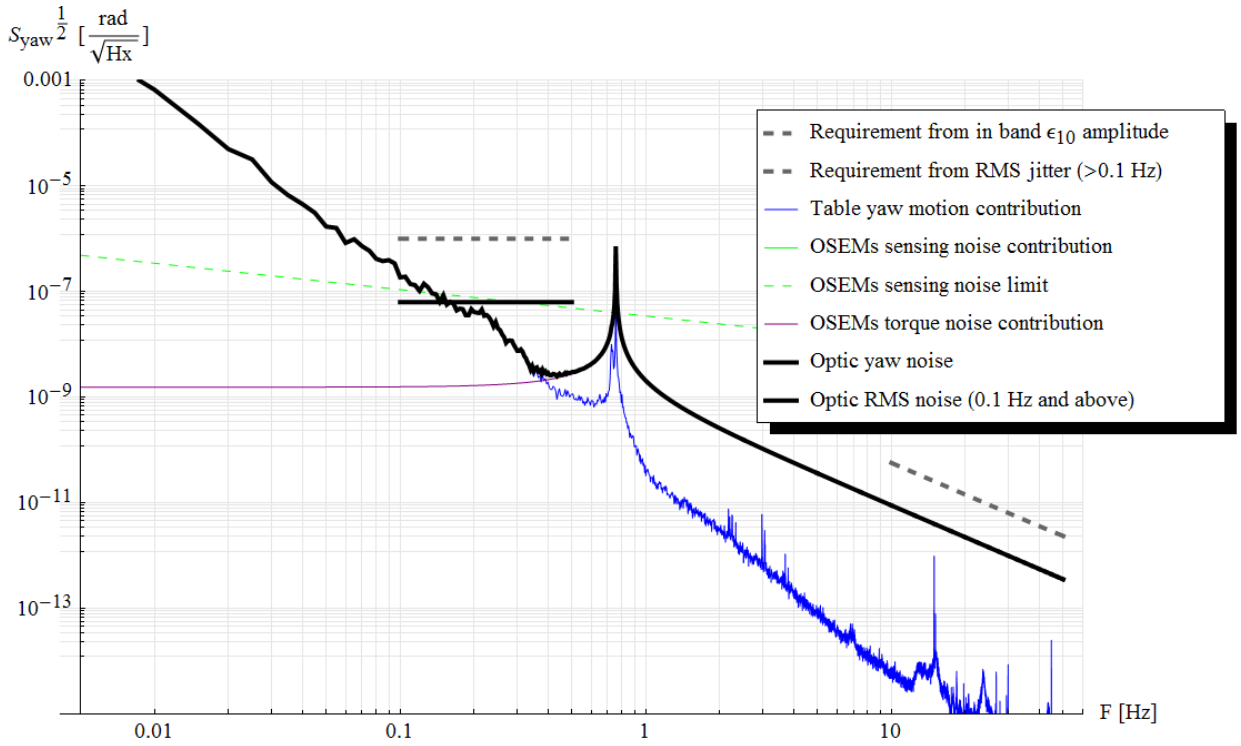

Figure 22. Projected yaw noise calculated using the Mathematica model with the control loop gain Gw set to zero. Contributions from individual noise sources are also shown. The flat short lines represent the RMS noise value (solid) and requirement (dashed) for f > 0.1 Hz. Note that the value of the RMS in this case (gain = 0) is greatly underestimated (see text).

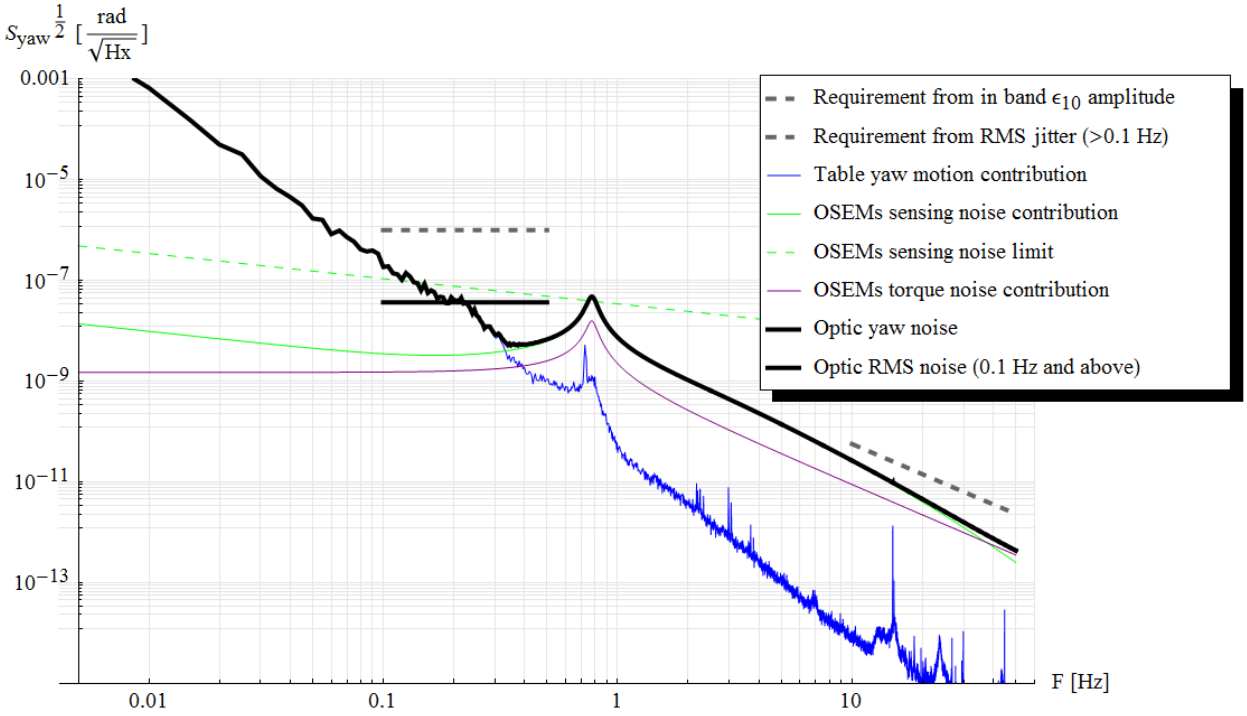

Figure 23. As Figure 22, but with the constant k in the control loop gain set to 0.5 (N m)/rad.

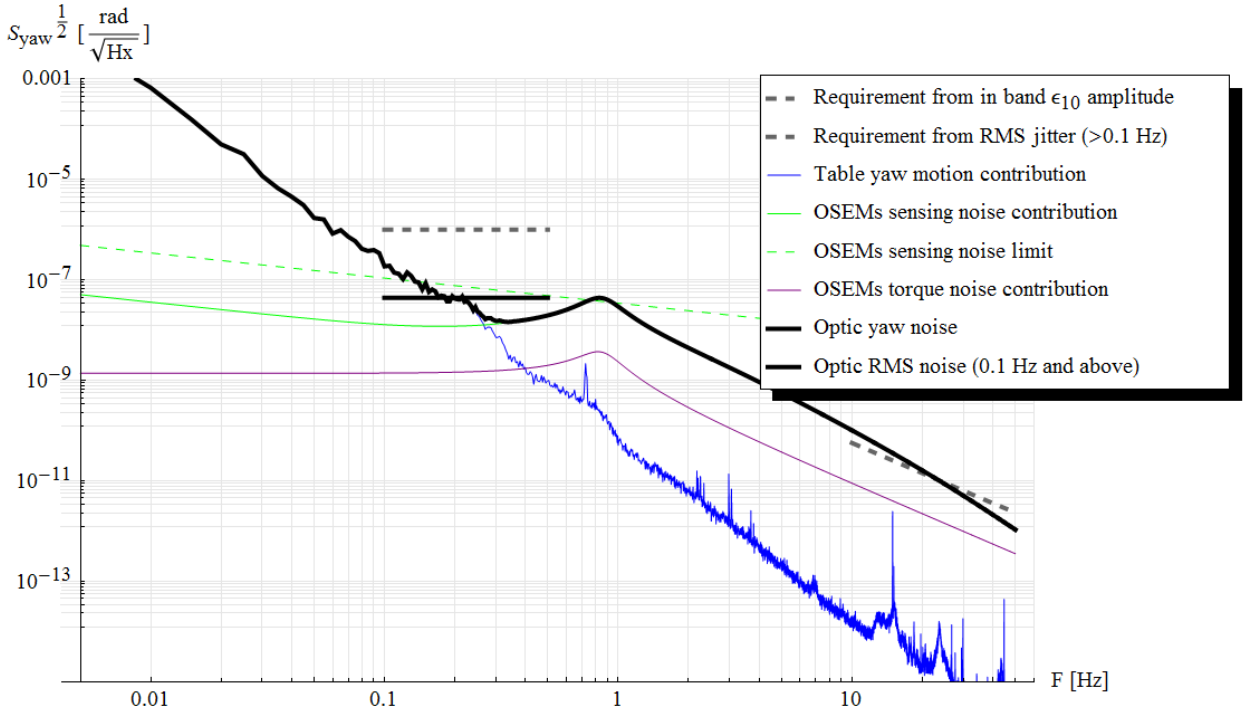

Figure 24. As Figure 22, but with the constant k in the control loop gain set to 2 (N m)/rad.

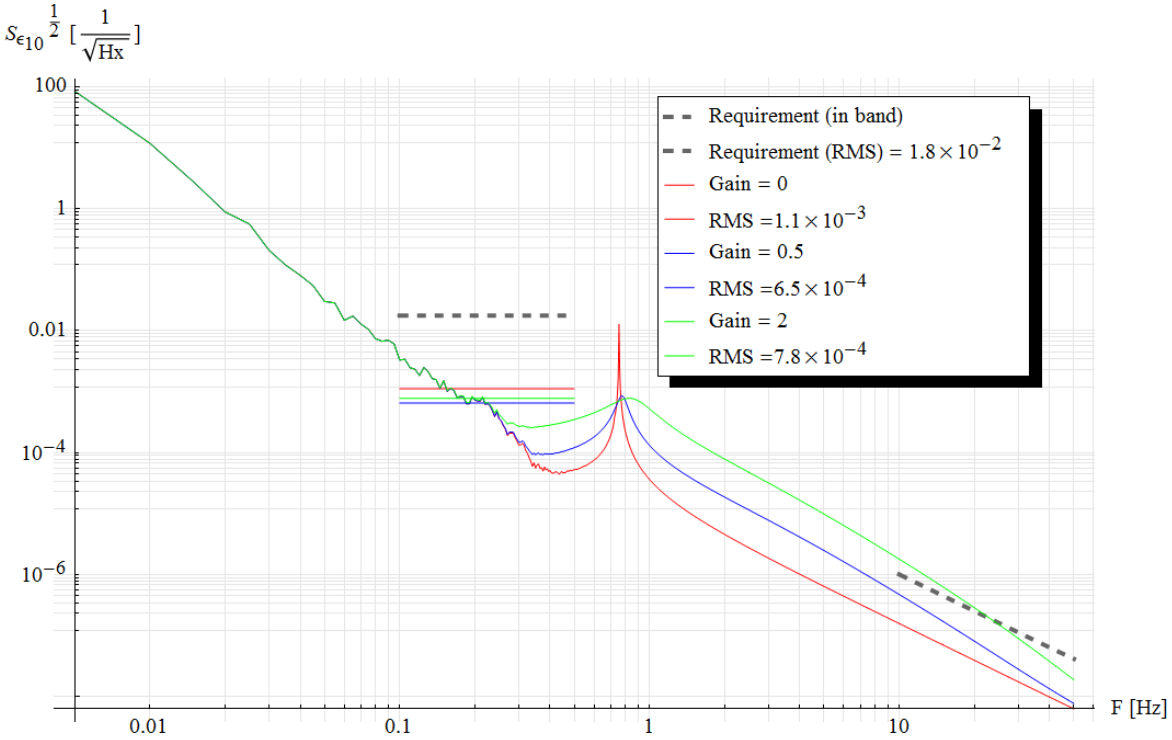

Figure 25. A comparison of the total TEM10 amplitude noise spectra due to the yaw motion of the optic. The colors represent the three different gain settings shown in previous figures. Note that the value of the RMS in the case of gain = 0 is greatly underestimated (see text).

2.3.7 X noise

Figure 26 illustrates the noise model for the x DoF. It is almost identical to the one for the pitch, as identical are the number and type of noise sources and coupling.

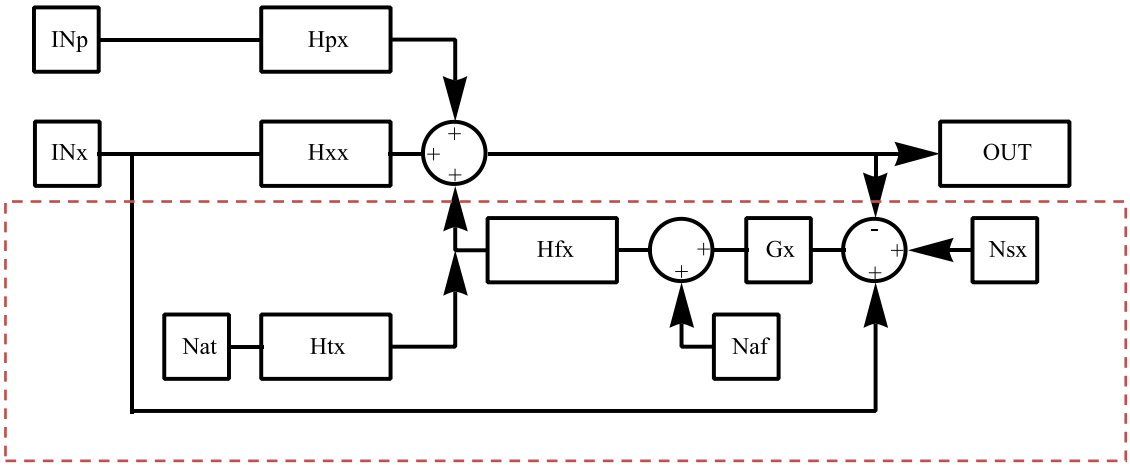

Figure 26. Schematics of the noise model for the x degree of freedom. See caption of Figure 16 and corresponding text for details.

New abbreviations have a straightforward meaning:

- Hpx: transfer function between suspension pitch and x motion of the optic
- Hxx: transfer function between suspension x motion and x motion of the optic
- Hfx: transfer function between force applied on the optic along the x axis and x motion of the optic
- Htx: transfer function between torque applied to the optic (y component), and x motion of the optic
- Naf: force noise coming from the AOSEMs array
- Nat: torque noise coming from the AOSEMs array
- Nsx: x sensing noise of the AOSEMs array
- Gx: gain of the control loop (for the x DoF)

The output is:

$$\frac{\mathrm{Hpx}}{1+\mathrm{Gx\,Hfx}}\mathrm{INp}+\frac{(\mathrm{Gx\,Hfx}+\mathrm{Hxx})}{1+\mathrm{Gx\,Hfx}}\mathrm{INx}+\frac{\mathrm{Hfx}}{1+\mathrm{Gx\,Hfx}}\mathrm{Naf}+\frac{\mathrm{Htx}}{1+\mathrm{Gx\,Hfx}}\mathrm{Nat}+\frac{\mathrm{Gx\,Hfx}}{1+\mathrm{Gx\,Hfx}}\mathrm{Nsx}$$

And the input noise sources, as well as the control loop gain function, have been assumed as for the pitch

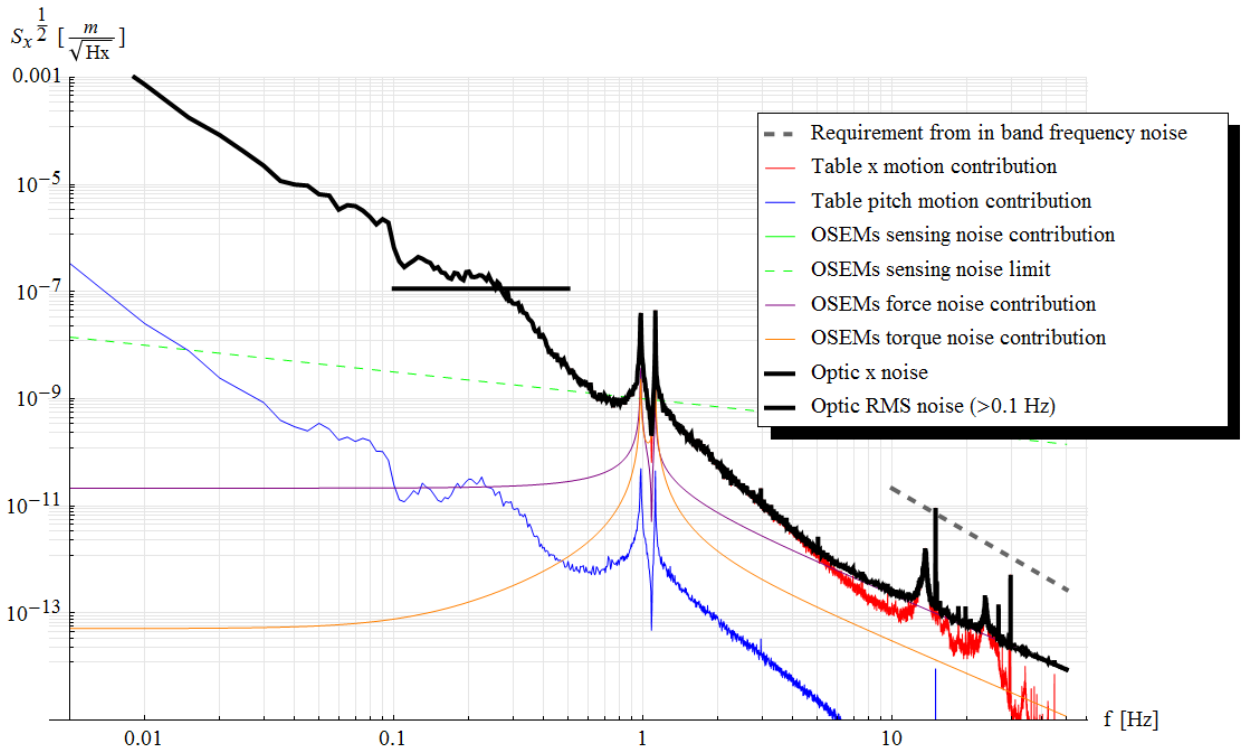

Figure 27. Projected x noise calculated using the Mathematica model with the control loop gain Gx set to zero. Contributions from individual noise sources are also shown. The flat solid short line represents the RMS noise value for f > 0.1 Hz. Note that the value of the RMS in this case (gain = 0) is greatly underestimated (see text).

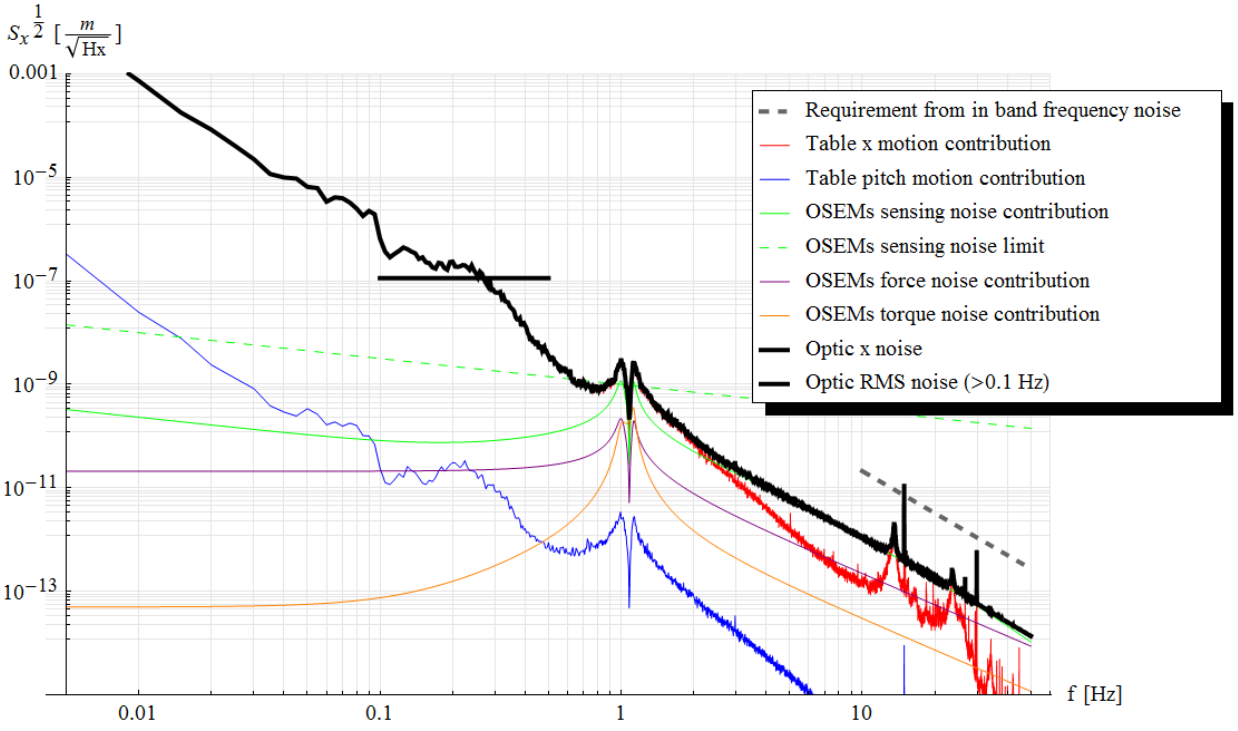

Figure 28. Figure 27, but with the constant k in the control loop gain set to 10^3 N/m.

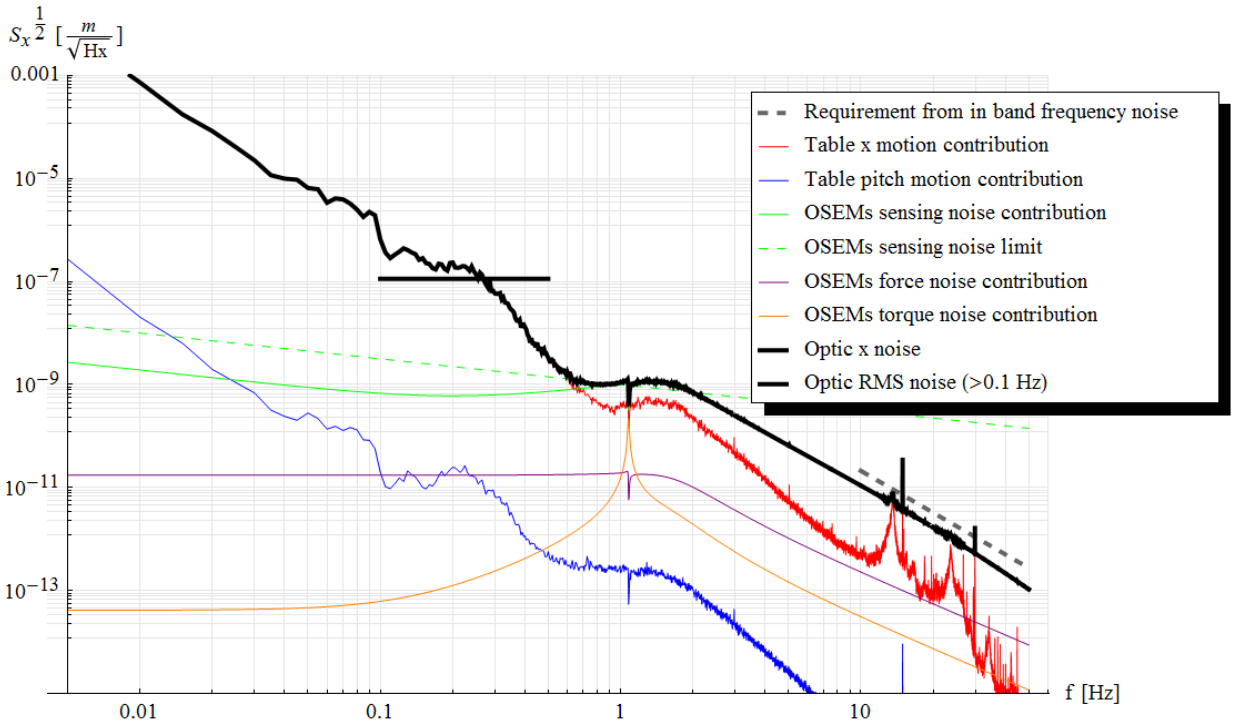

Figure 29. Figure 27, but with the constant k in the control loop gain set to 10^4 N/m.

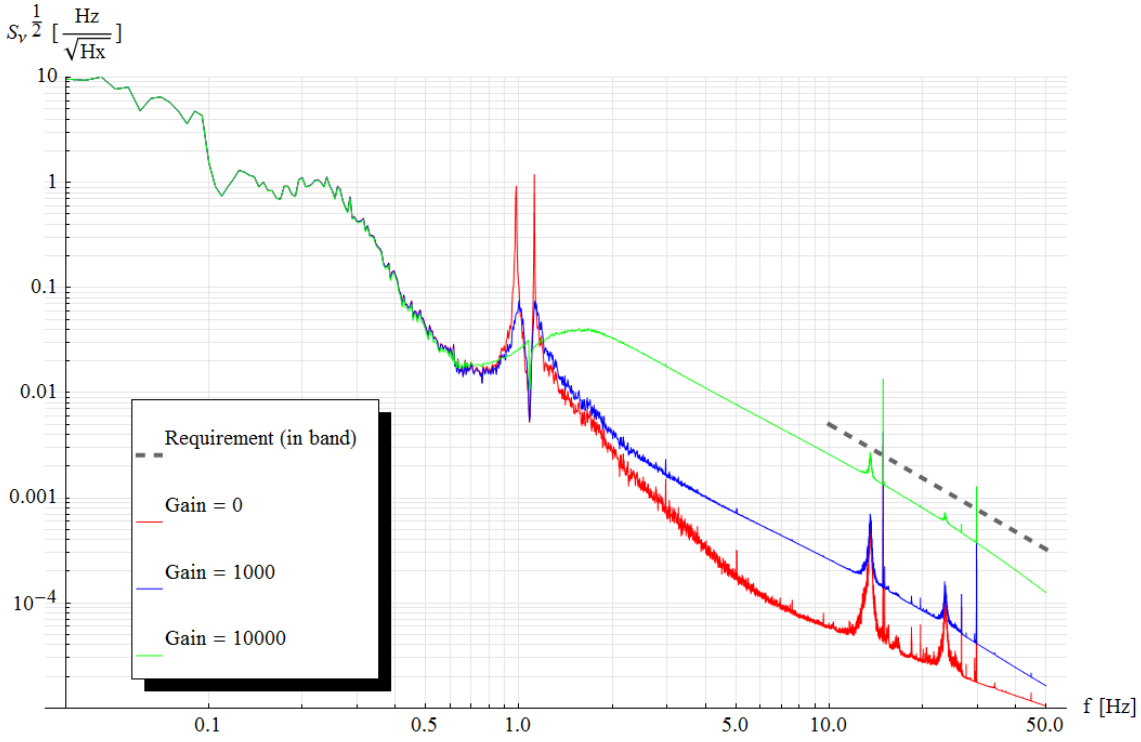

Figure 30. A comparison of the total frequency noise spectra due to the x motion of the optic. The colors represent the three different gain settings shown in previous figures. Note that the value of the RMS in the case of gain = 0 is greatly underestimated (see text).

3 Testing

To provide some validation to the Mathematica model, the fundamental resonant frequencies have been measured for all the six normal modes. In addition, the quality factors Q of the modes involving DoF that are not actively controlled by the AOSEMs have been measured to assess the effectiveness of the passive eddy current dampers.

3.1 Test setup

Three different test setups were necessary to measure all 6 normal modes. They are briefly explained in the following paragraphs.

3.1.1 Pitch, yaw and x

To measure the yaw and the two pitch/x normal modes we used a combination of two optical levers reflecting on the same face of the suspended optics from opposite sides, and coming from opposite directions. The setup is illustrated in Figure 31.

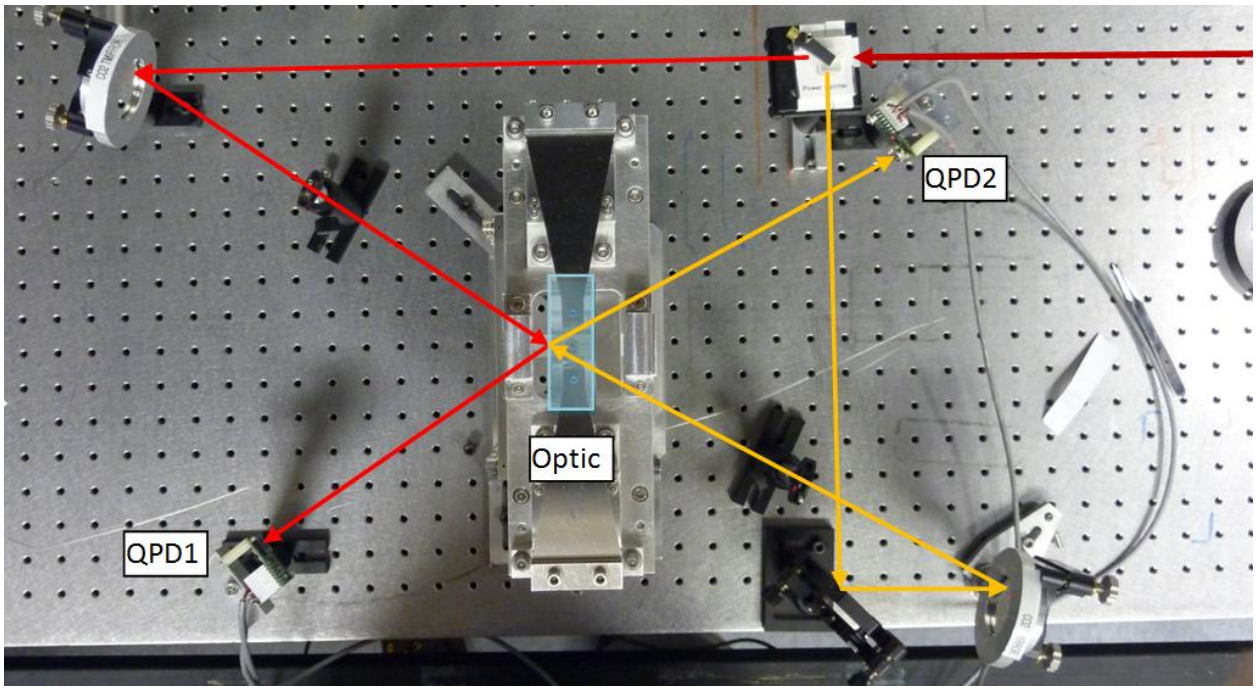

Figure 31. A top view of the experimental setup to measure pitch/x and yaw modes. The suspension is visible in the center, with the approximate size and position of the optic indicated by the light blue box. The arrow shows the laser paths to the two QPDs.

Calling H1, H2, V1 and V2 the horizontal and vertical difference channels of the QPD 1 and 2 respectively, the following combination can be formed:

- (H1+H2)/2: proportional to the x displacement of the optic
- (H1-H2)/2: proportional to the yaw motion of the optic
- (V1+V2)/2: proportional to the pitch of the optic. Note that because of the nominally null angle of incidence in the vertical plane, V1 and V2 can be independently taken as

proportional to the pitch of the optic. However, averaging them allows for reduction of noise and rejection of second order couplings with the optic x displacement.

Forming these combinations is not strictly necessary to measure the resonance frequencies. However, being these frequencies quite close one to the other, it helped ensuring that we were associating the correct resonant mode to each peak visible in the spectrum (by observing that it was the only one surviving in the appropriate combination of signals).

The resonant frequencies were obtained by fitting the appropriate peaks in the power spectrum.

3.1.2 Bounce and 2nd roll/y mode

The bounce mode is clearly visible by measuring the z position of the optics. However, the highest roll/y mode, primarily composed of a rotation of the optic around the optical axis, can also be observed by measuring the z coordinates of points that are away from the optical axis. To measure both modes we set up two shadow sensor on opposite sides of the optic holder, using the upper edges of the wire clamps as flags as illustrated in Figure 32.

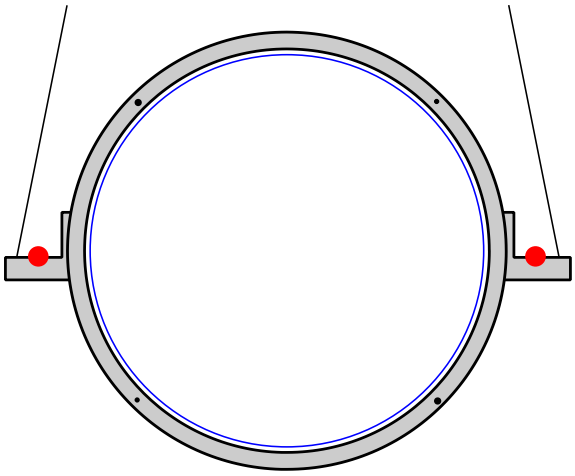

Figure 32. A schematic front view of the suspended assembly. The two red dots represent the laser beams that, coming from the direction of the observer hit two photodetectors behind the assembly. As you can see, they are partially blocked by the wire clamps, and the amount of power going to the photodetector depends on the z coordinates of the edges of the wire clamps. The signals coming from the detectors will be in phase when the optic bounces, and in anti-phase when it rolls.

The two modes can be separated by taking these two combinations of signals:

- (P1+P2)/2: proportional to the bouncing mode
- (P1-P2)/2: proportional to the highest roll/y mode

3.1.3 1st roll/y mode

Contrary to the highest roll/y mode, the lowest one implies primarily a translation of the optic in the y direction. To measure it, we moved the beams of the shadow sensors on the vertical edges of the wire clamps, as illustrated in Figure 33. The difference between the signals coming from the detectors can be taken as a measure of the y displacement of the optic.

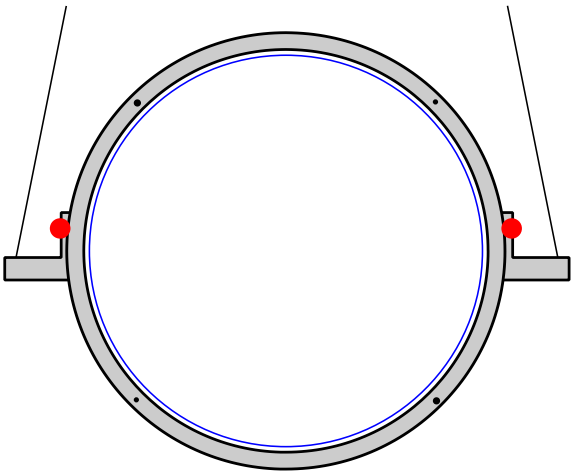

Figure 33. A schematic front view of the suspended assembly. The two red dots represent the laser beams that, coming from the direction of the observer hit two photodetectors behind the assembly. As you can see, they are partially blocked by the wire clamps, and the amount of power going to the photodetector depends on the y coordinates of the edges of the clamps. When the optic moves in the y direction, it creates two opposite signals on the detectors.

3.2 Test results

The resonant frequencies of the various modes were measured by fitting the power spectra of the relevant signal. Table 4 reports the measured values and those obtained from the model. Note that the frequencies have been measured with no damping in place to be directly comparable with those obtained from the model.

Table 4. Measured and calculated resonant frequencies of normal modes

Mode name	***Value from the model***	***Measured Value***
fPitch1	0.98 Hz	0.95 Hz
fPitch2	1.12 Hz	1.04 Hz
fYaw	0.76 Hz	0.80 Hz
fBounce	7.19 Hz	6.14 Hz
fRoll1	1.00 Hz	1.00 Hz
fRoll2	10.63 Hz	8.97 Hz

Except for the bounce and the higher roll/y modes, the discrepancies are small in all the modes, and can be easily explained with small errors in the model's parameters (machining and/or assembling tolerances, material properties, small errors in the moment of inertia calculated using SolidWorks).

We observe that the bounce and higher roll/y modes are the only ones that involve a significant blades' bending. Both frequencies are smaller than the expected values by about 15%; moreover by adjusting the spring value of the blades in the model to match the bounce frequency, we also get a

roll frequency close to the measured value (9.06 Hz). This suggests that the actual blade stiffness is smaller than expected by about 25%. The reason for this is not clear and has not been further investigated yet. However, we did check that the blades were not yielding noticeably after a few weeks under load.

For the DoF that are not actively controlled by AOSEMs, nominally y, z and roll, passive damping is obtained via eddy current dampers as described in LIGO-T1000338. The quality factors were measure by observing several ring-downs, and fitting an exponential decay to the signal demodulated at the oscillation frequency (that also provided a very precise way of measuring the oscillation frequency checking the demodulation to maintain the correct phase throughout many oscillations). Measured values with and without dampers in place are reported in Table 5.

Table 5. Measured quality factors and frequencies with damping

DOF	***Q no damping (in air)***	***Q with damping***	***F with damping***
Roll1 (around optic axis)	6000 ± 1000	74 ± 2	1.02 Hz
Roll2 (lateral swing)	500 ± 25	33 ± 3	8.98 Hz
Bounce	420 ± 20	43 ± 3	6.12 Hz